TWO-COLOR SPECTROSCOPIC STUDIES OF MERCURY

By

WILFREDO RESTO-OTERO

A DISSERTATION PRESENTED TO THE GRADUATE SCHOOL
OF THE UNIVERSITY OF FLORIDA IN PARTIAL FULFILLMENT
OF THE REQUIREMENTS FOR THE DEGREE OF
DOCTOR OF PHILOSOPHY

UNIVERSITY OF FLORIDA

1993

Copyright 1993

by

Wilfredo Resto-Otero

A mis padres, Darío y Virginia, y a mi esposa, Mildred.

ACKNOWLEDGEMENTS

I would like to thank Dr. James D. Winefordner for his financial support and professional advice and guidance, which made possible the completion of this work.

I also want to thank all the past and present members of the group for their friendship and help. In particular, I would like to thank Drs. Norma Ayala and Edison Becerra, who made my integration into the group and Gainesville more pleasant.

I would like to thank Drs. Nicolo Omenetto, Ben Smith, Giuseppe Petrucci, Raul Badini, and Denis Boudreau and Mr. Dennis Hueber for their help and the helpful discussions through the course of this work.

I would also like to thank all the hispanic members of St. Augustine Church, especially Mrs. Maggie Rodriguez, the past and present choir members and their loving directors, the Rodriguez family, who on more than one occasion have been the source of strength and spiritual support during difficult moments.

Finally, I would like to thank all my friends and the members of my family, especially to my in-laws, Mr. Javier Barreto and Mrs. Amelia Velazquez, and Ms. Lymari Montalvo, who with their care and loving have made me feel closer to home.

TABLE OF CONTENTS

ACKNOWLEDGEMENTS iv

LIST OF TABLES viii

LIST OF FIGURES x

ABSTRACT xiv

CHAPTERS

1 INTRODUCTION 1

General Remarks 1
Types of Fluorescence 2
Lasers as Excitation Sources 2
LEAFS Noise Sources 7
Concomitant Scatter 7
Stray Light 7
Atom Cell Emission 8
Molecular Fluorescence 8
Non-Analyte Atomic Fluorescence 8
Fluorescence Flux Expressions 9
Optical Saturation 9
Electrothermal Atomizers and Collection of Fluorescence 15
Importance of Mercury Determination 20
Methods for the Determination of Mercury 23
Mercury Spectroscopy 23

2 COOPERATIVE PROCESSES AND AMPLIFIED SPONTANEOUS EMISSION 33

A Question of Terminology 33
Coherence Brightening and Mirrorless Lasers 34
Normal Dicke Superradiance 35

Incoherently Prepared Dicke Superradiance 38
Optical Extensions of Dicke Superradiance 41
Superfluorescence 44
Amplified Spontaneous Emission 48
Introduction 48
Saturation 55
Temporal and Spatial Output 55
Cooperative Processes in Mercury 55

3 RATE EQUATIONS APPROACH 59

Introduction 59
Theoretical Considerations 60
Mercury Rate Equations 65

4 EXPERIMENTAL 72

Laser Excited Atomic Fluorescence Spectrometry 72
Instrumentation and Operational Parameters 72
Elimination of Mercury Loss 79
Determination of the Instrumental Limit of Detection 80
Calibration Curves 83
Amplified Spontaneous Emission 83
Instrumentation and Operational Parameters 83
Vapor Cells 86
Saturation Curves 93
ASE Dependence on Number Density of Mercury 93
ASE Dependence on Type of Buffer Gas 97
ASE Dependence on Nitrogen Gas Pressure 98

5 RESULTS AND DISCUSSION 101

Laser Excited Atomic Fluorescence Spectrometry 101
Elimination of Mercury Loss 101
Determination of the Instrumental Limit of Detection 102
Calibration Curves 111
Amplified Spontaneous Emission 119
Saturation Curves 119
ASE Signal Dependence on Mercury Number Density 124
ASE Signal Dependence on Type of Buffer Gas 135
ASE Signal Dependence on Nitrogen Pressure 138
Rate Equations Approach 138

6 CONCLUSIONS AND FUTURE WORK 150

APPENDICES

A COMPUTER LISTING OF BASIC PROGRAM USED FOR THE NUMERICAL SOLUTION OF THE RATE EQUATIONS 152

B COMPUTER LISTING OF BASIC PROGRAM USED FOR THE CALCULATION OF INSTRUMENTAL NOISE FOR LEAFS-ETA 155

C MODIFICATIONS TO COMPUTER PROGRAM LISTED IN APPENDIX A 157

REFERENCE LIST 158

BIOGRAPHICAL SKETCH 162

LIST OF TABLES

TABLES

1-1	Pump laser characteristics	6
1-2	Mercury toxic effects	21
1-3	Summary of EPA regulations for mercury	22
1-4	Different techniques for the determination of mercury	24
1-5	List of oscillator strengths, Einstein spontaneous emission coefficient, ΔS, ΔL, ΔJ for some mercury transitions.	25
2-1	Summary of initial conditions and characteristics of Dicke superradiance.	42
2-2	Summary of initial conditions and characteristics for incoherently prepared Dicke superradiance	43
2-3	Summary of initial conditions and characteristics for superfluorescence	49
3-1	List of parameters used for the development of the rate equations for mercury.	70
5-1	Instrumental limits of detection for LEAFS-ETA determination of mercury	109
5-2	Comparison of results for mercury determination with different techniques	110
5-3	Results of the Student t-test comparing the results of noise calculations made by a computer and manually made	112
5-4	Buffer gas effect on ASE signal relative to that of =500 torr of N_2	136

5-5 ASE signal dependence on type of buffer gas in the furnace. The signal is relative to the one for argon gas 137

LIST OF FIGURES

FIGURES

1-1 Types of fluorescence a) resonance fluorescence b) non-resonance fluorescence c) multiphoton fluorescence. 4

1-2 Typical saturation curve for atomic fluorescence 12

1-3 Fluorescence collection using the front surface illumination arrangement. 17

1-4 Fluorescence collection using the transverse illumination arrangement. 19

1-5 Mercury partial energy level diagram showing scheme-I as referred on text. 28

1-6 Mercury partial energy level diagram showing scheme II as referred on text 30

1-7 Mercury partial energy level diagram showing scheme-III as referred on text 32

2-1 Figure showing a normal Dicke superradiant medium 37

2-2 Different steps for incoherently prepared Dicke superradiance. a) spontaneous emission b) the spontaneous emission induced a dipole creating some polarization of medium c) superradiant pulse 40

2-3 Figure showing the different steps for superfluorescence. a) spontaneous emission b) the spontaneous emission induced a dipole creating some polarization of medium c) superradiant pulse 46

2-4 Representation of an amplified spontaneous emission medium 52

2-5 Mercury partial energy levels diagram showing pumping scheme used by Djeu for the opticaly pumped mercury-nitrogen laser ... 58

3-1 Energy levels diagram of the system used in the text. ... 62

3-2 Partial energy diagram of mercury showing the different excitation and deexcitation processes ... 67

4-1 Schematic diagram of the optical layout. The furnace and the mercury cell can be interchangeably placed in the optical path ... 74

4 2 Partial energy diagram for mercury ... 78

4-3 Graphite furnace temperature program ... 82

4-4 Schematic diagram of the optical layout for the amplified spontaneous emission experiments ... 85

4-5 Cell design I ... 88

4-6 Mercury vapor cell II, designed to allow cooling and heating ... 90

4-7 Mercury vapor cell III In this design the mercury is kept in a different compartment of the cell ... 92

4-8 Schematic diagram of the cooling and heating system ... 95

4-9 Schematic diagram of vacuum system ... 100

5-1 LEAFS-ETA signal for mercury during the furnace program The figure shows the mercury loss during the drying step ... 104

5-2 LEAFS-ETA signal for mercury, with Pd as matrix modifier, and modifications to the furnace program This clearly shows that the problem of mercury loss during the drying step was eliminated ... 106

5 3 Typical signals of the LEAFS ETA system for three mercury standards analyzed in duplicate ... 108

5-4 Calibration curves for λ_{01}=546.1 nm and λ_{02}=407.8 nm. The stray light noise level is for the measurement at λ_{01}=546.1 nm 114

5-5 Calibration curve for λ_{01} = 546.1 nm. The line is the regression as calculated by the graphing program. The last two points show the deviation due to ASE 116

5-6 Schematic diagram of the collection of fluorescence and ASE. 118

5-7 Saturation curve for the first transition at λ_1 = 253.7 nm. The line is the regression as calculated by the graphing program, and the error bars are $\pm\sigma$ of the triplicate measurement 121

5-8 Saturation curve for the second transition at λ_1 = 435.8 nm. The line is the regression as calculated by the graphing program. The error bars are $\pm\sigma$ of the triplicate measurement. 123

5-9 ASE signal dependence on mercury number density, with 760 torr of argon as buffer gas. (cell II) 126

5-10 ASE signal dependence on mercury number density for nitrogen at = 500 torr as buffer gas. (cell-I) 128

5-11 ASE signal dependence on number density for argon at 760 torr as buffer gas in the graphite furnace 130

5-12 Simplified mercury energy level diagram. Refer to text for explanations of simbols. 132

5-13 ASE signal dependence (relative to the signal one at 760 torr) on nitrogen pressure. The dashed line represents the absorption factor, as calculated by a Math-Cad 140

5-14 Theoretical saturation curve for the first transition at λ_{01} = 546.1 nm, as calculated by the rate equations approach. The population of level four had been normalized to the total number density 142

5-15 Theoretical saturation curve for the second transition at λ_{ne} = 435 8 nm, as calculated by the rate equations approach The population of level four had been normalize to the total number density 144

5-16 Comparison of the experimental saturation curve of the first transition for ASE, with the theoretical curve calculated by the rate equations approach 147

5-17 Comparison of the experimental saturation curve of the second transition for ASE, with the theoretical curve calculated by the rate equations approach 149

Abstract of Dissertation Presented to the Graduate School
of the University of Florida in Partial Fulfillment of the
Requirements for the Degree of Doctor of Philosophy

TWO-COLOR SPECTROSCOPIC STUDIES OF MERCURY

By

Wilfredo Resto-Otero

December 1993

Chairperson James D Winefordner
Major Department Chemistry

Mercury determination using laser excited atomic fluorescence with electrothermal atomization (LEAFS-ETA) has been obtained The scheme used is a two-step excitation, with λ_1 = 253.1 nm and λ_2 = 435.8 nm. Direct fluorescence is observed at 546 1 nm The practical limit of detection (LOD) obtained was 9 picograms, 1 parts per billion (ppb) with a 10 μL injection The linear dynamic range (LOR) is three orders of magnitude (from 1 ppb to 1 ppm) and is limited by the nonlinearity of the amplified spontaneous emission (ASE) process occurring at higher concentrations In order to extend the LDR, indirect fluorescence is measured using the less sensitive emission line at 407 8 nm. This scheme has a higher LOD and an LDR of at least three orders of magnitude. It can be used for concentrations of one part per-million and up, extending the LDR of the technique LEAFS-ETA is a novel and promising method for the determination of mercury.

For the first time ASE was observed for mercury vapor cell using pulsed excitation. The ASE at 546.1 nm is observed for concentrations higher than one ppm in the furnace and number densities $> 10^{13}$ cm^{-3} in mercury vapor cells using nitrogen and argon as buffer gases. The saturation curves for the ASE were measured for both wavelengths of excitation, showing both wavelengths, a square dependence on the energy of the respective laser. The dependence of the ASE on the number density is exponential for lower number densities, with an abrupt threshold followed by a plateau due to saturation of the ASE gain.

CHAPTER 1
INTRODUCTION

General Remarks

Atomic fluorescence was studied by physicists in the late nineteenth and early twentieth century, who observed fluorescence in flames and cells for several elements Atomic fluorescence was used by Alkemade and Milatz (1) to study physical and chemical processes in flames In 1962, they suggested that atomic fluorescence could be used for analytical purposes This suggestion was followed by Winefordner and Vickers (2), who in 1964 proposed and showed the use of atomic fluorescence in flames as a new analytical method Extensive studies and refinement were carried out by Winefordner's and West's groups after 1964

Due to the nature of atomic fluorescence and the experimental setups, the power detected is usually a 10^{-4} to 10^{-9} fraction of the excitation radiant power. Thus, most of the initial research in atomic fluorescence was in the development of intense sources (3) The introduction of lasers as sources has been a major improvement in the source intensity problem, leaving room for development of new applications for atomic fluorescence. The following is a discussion of some important aspects of atomic fluorescence, the use of lasers as excitation sources and the application of laser-excited atomic fluorescence spectrometry (LEAFS) to the determination of mercury.

Types of Fluorescence

There are several types of fluorescence. Some of them are resonance fluorescence, nonresonance fluorescence, and multiphoton fluorescence. In resonance fluorescence, the lower and upper levels involved in the excitation and emission processes are the same, thus the excitation and emission wavelengths are the same. For nonresonance fluorescence, the lower and upper levels involved in the excitation and emission processes are different, so that the wavelength of excitation is different from the emission wavelength. When the same upper level is involved in the excitation and emission, it is known as direct-line fluorescence. If different upper levels are involved in the excitation-emission process, it is known as stepwise fluorescence. In multiphoton fluorescence, two or more photons of the same or different wavelength excite the atom which then emits a photon of different wavelength. These types of fluorescence transitions are shown in Figure 1-1.

Lasers as Excitation Sources

The ideal excitation source for atomic fluorescence would be stable, intense, and tunable for all elements. It is difficult to find a source with all these characteristics. Some conventional sources that have been used for atomic fluorescence are hollow cathode lamps, electrodeless discharge lamps, and metal vapor discharge lamps. Although conventional sources are more frequently used, lasers are better sources because they can provide irradiances several orders of magnitude higher than conventional sources. The laser system should be able to generate wavelengths to probe

Figure 1-1. Types of fluorescence. a) resonance fluorescence, b) nonresonance fluorescence, c) multiphoton fluorescence

1
0
a

2
1
0
b

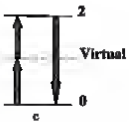
2
Virtual
0
c

atoms with sensitive lines almost anywhere in the visible and ultraviolet spectrum. The only laser systems that approach the ideal source are the dye lasers pumped by nitrogen, excimer or Nd YAG lasers (4). Because dye lasers can only lase at wavelengths longer than that of the pump laser, the lower the pump laser wavelength the more efficient it will be. A comparison of different pump lasers used for atomic fluorescence is shown in Table 1-1. Dye lasers are based upon absorption of radiation from the pump laser; dye lasers lase over a band of wavelengths characteristic of each dye. These lasers are tunable over a range of tens of nanometers, so several dyes are needed to cover the wavelengths from 320 to 900 nm.

To obtain more useful wavelengths from 190 to 320 nm, frequency conversion techniques are needed, including frequency doubling and sum frequency generation. In frequency doubling, two incident laser photons of frequency ν_1 are absorbed by a non-centrosymmetric crystal in the ground state, when the excited crystal returns to the ground state, a single photon of frequency ν_n ($\nu_n = 2\nu_1$) is emitted. The fundamental principle governing these phenomena is called second harmonic generation (5-6). For sum frequency generation, two laser beams having different frequencies ν_1 and ν_2 are combined in a noncentrosymmetric crystal to generate an emission beam with a frequency ν_m, equal to the sum of the frequencies of the two incident beams (7). Such conversion techniques give versatility to laser systems, allowing them to cover a wavelength range from 190-900 nm and making possible the probing of atoms almost anywhere in the visible and ultraviolet spectrum as required.

Table 1-1 Pump laser characteristics

Pump Laser	Output Wavelength (nm)	Pulse Energy* (J)	Repetition Rate* (Hz)
Nitrogen	337	0 01	100
XeCl	308	1	1000
Nd YAG	1064	10	50
Cu vapor	511	25	10000

* Maximum values available with commercial lasers They are not obtained simultaneously.

From reference 4.

Laser excited atomic fluorescence spectrometry (LEAFS) with electrothermal atomization (ETA) has been shown to achieve limits of detection in the femtogram and subfemtogram range for several elements (4, 8-13). The theory of LEAFS has been widely studied and reviewed (14-25). Characteristics of LEAFS have been reviewed by Butcher et al. (4). Also, they discuss the factors affecting the calibration curves, such as self-absorption and prefilter and postfilter effects. Some of these characteristics and factors are discussed in the following sections of this chapter.

LEAFS Noise Sources

Concomitant Scatter

Concomitant scatter is the noise generated when the laser is scattered off particles introduced by the sample. This type of noise is most significant when involatile and undissociated matrices are analyzed. This type of noise can be minimized by using a narrow bandwidth laser with line width equal to or less than that of the absorption line width. In that case, there will be very little unabsorbable light and hence less light will be scattered.

Stray Light

Stray light is scattered light that does not originate from the sample itself. This type of noise occurs when the laser is scattered off particles in the atom cell (e.g., water in a flame), off the wall of an atom cell (e.g., furnaces) or off parts of the instrument

(e g., windows and lenses). This noise can also be minimized by using a narrow band laser, because there will be very little unabsorbable laser light

Atom Cell Emission

This type of noise generally increases with detection wavelength and with temperature of the atom reservoir For a flame, increasing the temperature will increase the background emission that is produced In the case of a furnace, increasing the temperature will increase the blackbody emission For the flame, it is not possible to separate the emission spatially from the fluorescence, but for the furnace, masking the cell walls of the tube is a possible way of minimizing background emission.

Molecular Fluorescence

Molecular fluorescence is generated by species present in the atom reservoir or in the sample In furnaces, molecular fluorescence can only originate from the sample because the atomization process occurs in an inert atmosphere. This type of noise can be minimized by avoiding cooler regions in the atom reservoir, thus avoiding molecule formation in this region.

Non Analyte Atomic Fluorescence

Non analyte atomic fluorescence is fluorescence due to overlapping of atom lines. This type of overlap increases with increasing laser line width, so it can be minimized by using a laser with a line width equal to or less than the atomic line width.

Fluorescence Flux Expressions

The total fluorescence flux, Φ_F (W), produced in a volume V by absorption path length l is given by:

$$\Phi_F = (\Phi_{\lambda m})_0 \, Y \, \alpha \tag{1-1}$$

where $(\Phi_{\lambda m})_0$ is the spectral radiant power (W m^{-3}) at the line center, α is the fraction absorbed, and Y is the fluorescence power yield (dimensionless) The fluorescence power yield is given by

$$Y = \frac{A_{ji}}{A_{ji} + k_j} \tag{1-2}$$

where A_{ji} is the Einstein coefficient of spontaneous emission (s^{-1}), and k_j is the collisional deactivation rate (s^{-1}). Substituting α in equation 1-1 for an optically thin conditions expression we have

$$(\Phi_F)_{n_i} \, l \to 0 = 8.82 \times 10^{-13} \lambda_m^2 \, (\Phi_{\lambda m})_0 \, Y \, n_i \, f_{ij} \, l \tag{1-3}$$

where the constant has units of m, λ_m is the wavelength of the transition (m), n_i is the number density (m^{-3}), f_{ij} is the oscillator strength (dimensionless), and l is the absorption path length (m)

Optical Saturation

An atomic system achieves optical saturation when the rate of stimulated absorption (s^{-1} m^{-1} nm J^{-1}), B_{ij}, equals the rate of stimulated emission (s^{-1} m^{-1} nm J^{-1}), B_{ji},

A saturation curve, a plot of fluorescence intensity versus source energy, is presented in Figure 1-2. This plot can be divided in two main regions. The first region is the linear region, where the plot has a slope of one, which is the case for fluorescence excited by conventional sources. The second region is the constant region, where the plot has slope of zero and the transition is considered to be saturated. Lasers have sufficient intensity to achieve saturation of many transitions.

The fluorescence flux Φ_F (W) is given by

$$\Phi_F = h\,\nu\,A_{ji}\,n_j\,V^{*} \tag{1-4}$$

where h is the Planck's constant (J s), ν is the frequency (s^{-1}), A_{ji} is the Einstein coefficient of spontaneous emission (s^{-1}), V^{*} is the volume of collected fluorescence (m^3), and n_j is the number density of the excited state (m^{-3}). Under steady-state conditions, the rate of absorption and the total rate of deactivation are balanced so that

$$\frac{B_{ij}(E_\lambda)_i n_i}{c} = [k_j + A_{ji} + \frac{B_{ji}(E_\lambda)_i}{c}]n_j \tag{1-5}$$

where k_j is the collisional deactivation rate (s^{-1}), c is the speed of light (m s^{-1}), n_i is the number density of the ground state (m^{-3}), and $(E_\lambda)_i$ is the spectral irradiance(W m^{-2} nm^{-1}). The spectral irradiance is given by

$$(E_\lambda)_i = \frac{\partial Q}{\partial t \partial S \partial \lambda} \tag{1-6}$$

where Q is the energy (J), t is the time (s), S is the area (m^2), and λ is the wavelength (m).

Using the definition of the spectral energy density $(U_\lambda)_i$, (J m^{-1} nm) is given by,

Figure 1-2 Typical saturation curve for atomic fluorescence

Slope = 0
Slope = 1
Log of Fluorescence Signal
Log of Source Energy

$$(U_\lambda)_i = \frac{(E_\lambda)_i}{c} \tag{1-7}$$

Substituting equation 1-7 into equation 1-5 we have:

$$B_{ij}\,(U\lambda)_i\,n_i = [k_j + A_{ji} + B_{ji}\,(U_\lambda)_i \tag{1-8}$$

B_{ij} and B_{ji} are related by the following equation:

$$B_{ij} = \frac{g_j}{g_i} B_{ji} \tag{1-9}$$

where g_j and g_i are the statistical weights of the states. Substituting equations (1-2) and (1-9) into equation (1-8), dividing by $B_{ji}\,(U_\lambda)_i$, substituting equation (1-7), and rearranging gives:

$$\frac{g_j n_j}{g_i n_i} = [1 + \frac{A_{ji} c g_j}{Y B_{ij} (E_\lambda)_i g_i}]^{-1} \tag{1-10}$$

$(E_\lambda^s)_i$ is the saturation spectral irradiance (W m^{-2} nm^{-1}), which is the spectral irradiance, $(E_\lambda)_i$, for which the fluorescence signal is 50% of its maximum value, and it is given by:

$$(E_\lambda^s)_i = \frac{A_{ji} c}{Y B_{ij}} \frac{g_j}{(g_i + g_j)} \tag{1-11}$$

Using the relation:

$$n_j = n_M (1 + \frac{n_0}{n_i}) \tag{1-12}$$

and combining it with equations (1-4), (1-10) and (1-11) we obtain:

$$\phi_F = h\nu A_{ij} V^* n_M \frac{g_i}{g_j + g_i} [1 + \frac{(E_\lambda^*)_0}{(E_\lambda)_0}]^{-1} \tag{1-13}$$

For low intensity sources such as conventional sources, $(E_\lambda)_0 << (E_\lambda^*)_0$ thus equation 1-13 becomes,

$$\phi_F = \frac{h\nu}{c} V^* n_M (E_\lambda)_0 Y B_{ij} \tag{1-14}$$

In this case, as shown in the saturation plot, the maximum fluorescence signal is not obtained. The mechanism of level population will be controlled by the quenching rate, and the fluorescence signal will be proportional to the laser energy and quantum efficiency. This is detrimental to any analytical measurement, because any fluctuation in the source intensity will introduce noise to the measurement.

For high intensity sources such as lasers, $(E_\lambda)_0 >> (E_\lambda^*)_0$, thus equation 1-13 becomes,

$$\phi_F = h\nu A_{ij} V^* n_M \frac{g_i}{g_j + g_i} \tag{1-15}$$

In this case, the maximum fluorescence signal is obtained, and the signal is independent of the quantum efficiency and laser intensity fluctuations. The mechanism of level population will be dominated by the coefficients of stimulated absorption and stimulated emission of the transition. Saturation conditions are desirable for analytical determinations because the fluorescence signal is the maximum and independent of laser intensity. Care should be taken, though, because the noise coming from scattered laser

light is proportional to the laser intensity over the whole energy range. The minimum laser intensity to saturate should be used so as to minimize the scattered signal.

Electrothermal Atomizers and Collection of Fluorescence

Several electrothermal atomizers, such as rods, cups, boats and tubes, have been used for LEAFS-ETA. Dittrich and Stärk (26) showed that the tube atomizer had better sensitivity and detection power due to a higher heating rate, a higher atomization efficiency, a longer atom residence time and a more homogenous temperature.

Several arrangements for collection of fluorescence radiation have also been used. Wei et al. (25) compared front-surface illumination (Figure 1-3) with the transverse arrangement (Figure 1-4) and concluded that the front-surface arrangement gave better limits of detection (LOD) because it had better illumination and collection efficiency. Also, front surface illumination has allowed the use of a commercially available atomizer without any modification. Detection has been made using both dispersive and nondispersive systems. A detailed comparison of the collection arrangements and detection approaches has been made by Wei et al. (25).

LEAFS-ETA combines the sensitivity and selectivity of laser atomic fluorescence with the performance of the commercially available electrothermal atomizer with excellent limits of detection and linear dynamic ranges. The major drawbacks are that there is no complete commercial instrument for LEAFS-ETA available, the laser system is expensive and complex, and the actual laser systems are unreliable.

Figure 1-3 Fluorescence collection using the front-surface illumination arrangement.

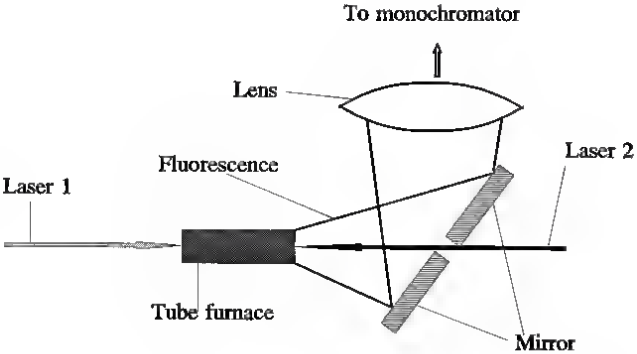
To monochromator
Lens
Laser 2
Fluorescence
Laser 1
Tube furnace
Mirror

Figure 1-4 Fluorescence collection using the transverse illumination arrangement.

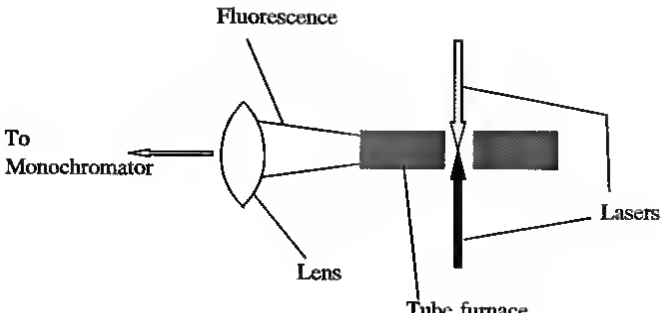
Fluorescence
To
Monochromator
Lasers
Lens
Tube furnace

Importance of Mercury Determination

The importance of mercury determination at ppb and sub ppb levels has increased in recent years due to environmental implications. A typical example is the documentation of mercury contamination in many lakes in Canada, Sweden, Finland and the United States (27). Some of these lakes contain fish with mercury levels that are a health risk to humans who consume them (28-29). Among some of the toxic effects of mercury are abdominal pain, kidney damage, severe nausea and vomiting, and death within ten days for a case of acute intoxication (30). For cases of chronic intoxication, spasms of the extremities and personality changes are among the toxic effects (30). A more complete list of the toxic effects of mercury is shown in Table 1-2. The Environmental Protection Agency (EPA) uses the guidelines set by several legislative acts that regulate, among others, mercury concentration in different matrices (31). For water, there is the Safe Drinking Water Act (SDWA), the Federal Water Pollution Control Act (FWPCA), and the Safe Drinking Water Amendments. The mercury maximum contaminant level for drinking water is 2 ppb. For solid and hazardous waste there is the Resource Conservation and Recovery Act (RCRA). The mercury maximum contaminant level for solid and toxic waste is 200 ppb. The Comprehensive Environmental Response, Compensation and Liability Act (CERCLA) sets other limits for contaminants. For example, the required limit of detection (LOD) for a laboratory that is performing EPA contracted determination of mercury is 0.2 ppb. These regulations are summarized in Table 1-3.

Table 1-2 Mercury toxic effects.

Acute Intoxication	Chronic Intoxication
Corrosive effects on skin and mucous	Inflammation of mouth and gums
Severe nausea and vomiting	Excessive salivation
Abdominal pain	Loosening of teeth
Bloody diarrhea	Kidney damage
Kidney damage	Muscle tremors
Death within 10 days	Jerky gaits
	Spasms of extremities
	Personality changes
	Depression
	Irritability
	Nervousness

From reference 30

Table 1-3. Summary of EPA regulations for mercury

Type of Regulation	Concentration (ppb)
MCL* for drinking water	2.0 ppb
MCL* for solid waste	200 ppb
MCL* for hazardous waste	200 ppb
CRDL** for contracted laboratories	0.20 ppb

* MCL = Maximum contaminant level

** CRDL = Contract required detection limit

From reference 31.

Methods for the Determination of Mercury

Mercury has been determined by atomic absorption-cold vapor (32), resonance ionization (33), fluorescence-cold vapor (34), atomic absorption with platinum-coated graphite tube (35), atomic absorption-electrothermal atomization (36), and inductively coupled plasma-mass spectrometry (37) Also, there is a review paper on several other atomic fluorescence methods (38) Some of these techniques have achieved limits of detection in the ppt range, with the drawback of a preconcentration step that results in a high absolute limit of detection. Some of them require larger sample volumes and long integration times A summary of these techniques is presented in Table 1-4

In the case of the two-step excitation LEAFS-ETA determination of mercury, the technique allows the direct determination of mercury in small sample volumes with limits of detection that can probably get as low as femtogram (ppt) range

Mercury Spectroscopy

In Table 1 5, the oscillator strengths, Einstein coefficients of spontaneous emission, ΔS, ΔL, and ΔJ are listed for the some mercury transitions. This table shows that the ΔS for the first transition is equal to one, making that transition forbidden

Because of this spectral characteristic of mercury, using a resonance fluorescence scheme involving the transition between the ground state 6^1S_0 level and the 6^3P_1 level is not the most sensitive approach because this transition is forbidden A two-step excitation scheme is the one alternative to a resonance excitation-fluorescence measurement

Table 1-4 Different techniques for the determination of mercury

Method*	LOD (fg)**	LOD (pptr)**	Observations (D / P)***	Reference
AA-CV	200,000	20	P	32
DRI	337	ND	P	33
FL-CV	5000	0 1	P	34
AA-Pt-ETA	30,000	0.6	P	35
AA ETA	25,000	500	D	36
ICP MS	ND	30	D	37

* AA = Atomic absorption
CV = Cold vapor
DRI = Double resonance ionization
FL = Fluorescence
ETA = Electrothermal atomization
Pt-ETA = Platinum coated graphite tube
ICP-MS = Inductively coupled plasma mass spectrometry

** ND = Not determined

*** D = Direct
P = Pre-concentration

Table 1-5 List of oscillator strengths, Einstein spontaneous emission coefficient, ΔS, ΔL, ΔJ for some mercury transitions.

Transition Wavelength (nm)	Oscillator Strength	Spontaneous Emission Coefficient (s^{-1})*	ΔS	ΔL	ΔJ
253.7	0.025	1.3×10^7	1	1	1
435.8	0.11	4.0×10^7	0	-1	0
546.1	0.15	5.6×10^7	0	-1	-1
404.7	0.13	1.7×10^7	0	-1	1
407.8	0.003	3.6×10^4	-1	-1	-1

* From reference 39.

The first possible two-step excitation scheme, scheme-I, is shown in Figure 1-5. In this scheme the first excitation at λ = 253 7 nm brings the atom to level $6^3P_1^0$, which is followed by an excitation at λ = 435 8 nm to level 7^3S_1. These excitations are followed by collisional deactivation to level $6^1P_1^0$, which then fluoresces at λ = 184 9 nm. The main disadvantages with this scheme are the fluorescecence wavelength requires the work to be done in an inert environment or in a vacuum, and coupling between the levels 7^3S_1 and $6^3P_1^0$ is not efficient.

The second excitation scheme, scheme-II, is shown in Figure 1-6. The first excitation is the same one used in scheme-I. The second excitation step is at λ = 407 8 nm, followed by radiative deactivation at λ = 1014 nm to level $6^1P_1^0$, followed by fluorescence at λ = 184 9 nm. Again, this scheme presents the disadvantage of requiring inert or vacuum working conditions.

Scheme-III, which is shown in Figure 1-7, presents a first excitation like that of schemes I and II, a second excitation like that of scheme I, and fluorescence at λ = 546 1 nm. This scheme seems to be convenient because it avoids the requirement of using vacuum or inert conditions for the determination.

Figure 1-5. Mercury partial energy level diagram showing scheme-I as referred in text.

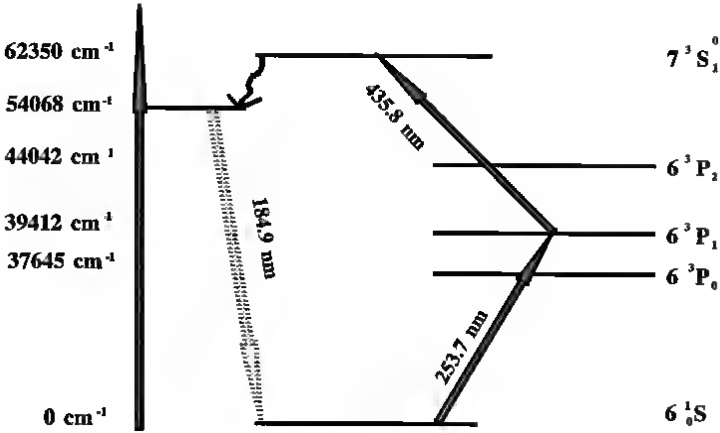
62350 cm-1
54068 cm-1
44042 cm-1
39412 cm-1
37645 cm-1
0 cm-1
184.9 nm
435.8 nm
253.7 nm
7 3 S1 0
6 3 P2
6 3 P1
6 3 P0
6 1 0 S

Figure 1-6 Mercury partial energy level diagram showing scheme-II as referred in text

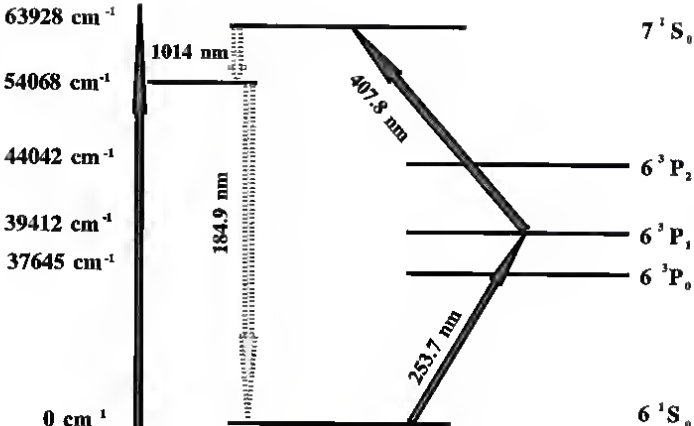
63928 cm-1
54068 cm-1
44042 cm-1
39412 cm-1
37645 cm-1
0 cm 1
1014 nm
184.9 nm
407.8 nm
253.7 nm
7 1 S0
6 3 P2
6 3 P1
6 3P0
6 1S0

Figure 1-7. Mercury partial energy level diagram showing scheme-III as referred in text

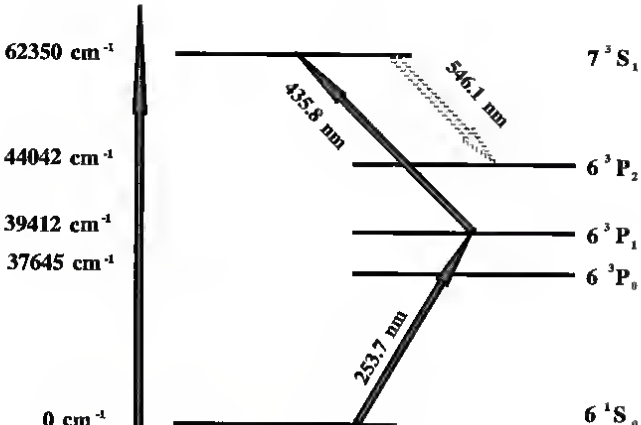
62350 cm-1
44042 cm-1
39412 cm-1
37645 cm-1
0 cm-1
435.8 nm
546.1 nm
253.7 nm
7 3S1
6 3P2
6 3P1
6 3P0
6 1S0

CHAPTER 2
COOPERATIVE PROCESSES AND AMPLIFIED SPONTANEOUS EMISSION

A Question of Terminology

From the theory of lasers (40), it is known that a collection of two-level atomic systems will emit electromagnetic radiation coherently, if the atoms are prepared in a way such that the individual atomic dipoles are oscillating at least partially in phase with each other. The radiation will have directional or spatially coherent properties determined by the relative phases with which the radiating atoms are initially set.

The cooperative processes can be divided in two major categories, the stimulated emission and the spontaneous emission. In the stimulated emission case, the cooperative process will result in a laser process. The spontaneous emission category can be divided into three different phenomena, normal Dicke superradiance, incoherently prepared Dicke superradiance, and superfluorescence.

The parameter C is known as the parameter that describes the cooperative behavior versus the one-atom behavior. It is given by:

$$C=\frac{\gamma_R}{2\gamma_a} \tag{2-1}$$

where γ_R is the cooperative decay rate (s^{-1}), and γ_s is the decay rate of a single atom(s^{-1}) For cases where $C << 1$, then the atoms emit independently from the other atoms. If $C >> 1$, then the system will evolve in cooperative behavior. Before the invention of the laser, and since the introduction of the concept of cooperation to spontaneous emission by Dicke (41) in 1954, cooperative processes have been an area of active research and controversy. Confusion has grown in the literature between the different cooperative processes. The terms superradiance (SR), superfluorescence (SF), amplified spontaneous emission (ASE), coherence brightening and mirrorless lasers have sometimes been use interchangeably and inconsistently in the literature. Some authors and books (40,42) have pointed out that this confusion is of semantic origin, and that the different types of cooperative effects can be all classified by their initial requirements, the nature of the cooperation and the characteristics of the emission. This chapter will discuss the different types of cooperative processes, as well as some introduction of amplified spontaneous emission processes for mercury.

Coherence Brightening and Mirrorless Lasers

Coherence brightening is the combination of spatial coherence with some spectral narrowing. This term does not have a very precise definition and has been observed in the literature for all of the cooperative processes.

The term mirrorless laser applies more to the process of amplified spontaneous emission and should be reserved for this very process only, and not to the more specialized phenomena such as superradiance and superfluorescence.

Normal Dicke Superradiance

In the usual treatment of spontaneous radiation, the radiation process of a molecule, is independent of other molecules. This assumption is made because the distance between the molecules is large and the interactions are weak, thus the probability of a molecule emitting a photon should be independent of photons emitted by other molecules. Dicke (38) stated that this model, though, cannot describe the dependence on the square of the concentration for a coherent spontaneous radiation system.

In his theory, the atomic medium as a whole, was treated as a single quantum mechanical system. The approach to the problem was to find the energy states representing correlated motions in the system, because spontaneous emission of coherent radiation will accompany transitions between those levels. Dicke treated the problem in a quantum mechanical, semiclassical and classical way. Also, he discussed the two principal methods of exciting coherent states, by absorption of photons from an intense radiation pulse or the emission of photons by the atoms. He calculated the effects of the two on the atomic system initially in equilibrium.

Dicke analyzed the situation where a large number of atoms contained in a small volume V, may all be oscillating with a high degree of coherence between the individual dipole oscillations, as shown in Figure 2-1. The macroscopic dipole moment within the volume will have the magnitude $N\mu_1$, where μ_1 is the oscillating dipole moment of a single atom, and N is the number of coherently oscillating atomic dipoles. The rate of coherent radiative power emission from this coherently prepared volume of atoms, will be proportional to the macroscopic dipole squared $(N\mu_1)^2$, that is different to the common

Figure 2-1. Figure showing a normal Dicke superradiant medium.

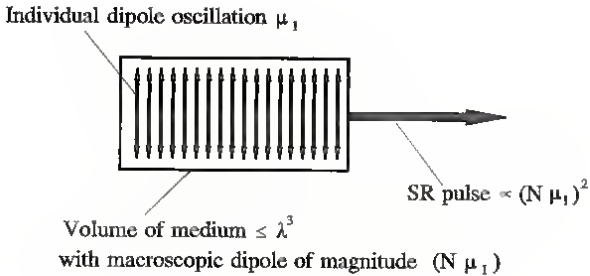
Individual dipole oscillation μ_1
SR pulse $\propto (N\,\mu_1)^2$
Volume of medium $\leq \lambda^3$
with macroscopic dipole of magnitude $(N\,\mu_1)$

and incoherent form of spontaneous emission, where the emission rate is proportional to the number of atoms, N. Also, the coherent emission of this small, coherently excited volume will emerge as a short pulse of radiation with a duration proportional to the inverse of the number of atoms (N^{-1}) rather than as an exponential decay with a lifetime, τ, independent of the number of atoms.

The atoms are locked together by the initial preparation, all in phase with each other, and by the strong coupling of all the atoms to each other through their common radiation field. This process, small-volume, coherently prepared emission, with strong initial coherence, is known as Dicke superradiance. Dicke superradiance can be observed in specially prepared low frequency magnetic resonance systems, but not in optical frequencies.

Incoherently Prepared Dicke Superradiance

In this case, consider a two-level system, with N number of atoms, incoherently excited, completely inverted, $N_1 = 0$ and $N_2 = N$, so that all the atoms are in their upper energy level to start with. In this case, there is no macroscopic polarization, because the quantum expectation value for the dipole oscillation of each individual atom is zero if the atom is entirely in level 1 or 2. Each atom in its upper level will begin to radiate spontaneously and incoherently Figure 2-2a, with a rate of A_{21}, where A_{21} is the Einstein coefficient of spontaneous emission. Such a system will emit normal fluorescence proportional to N.

Figure 2-2 Different steps for incoherently prepared Dicke superradiance. a) spontaneous emission b) the spontaneous emission induced a dipole creating some polarization of medium c) superradiant pulse

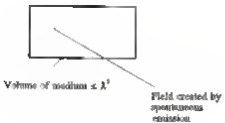
Volume of medium ≤ λ³
Field created by spontaneous emission

a

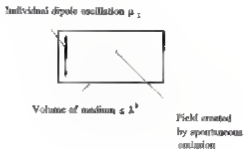
Individual dipole oscillation μ ;
Volume of medium ≤ λ³
Field created by spontaneous emission

b

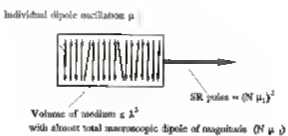
Individual dipole oscillation μ
SR pulse ∝ (N μ ;)²
Volume of medium ≤ λ³
with almost total macroscopic dipole of magnitude (N μ ;)

c

If N atoms are confined in a volume V such that V is smaller or equal to the emission wavelength cubed ($V \leq \lambda^3$), then coupling between the fields will occur, because of their overlapping radiation fields. The atoms, in this case will no longer radiate independently and incoherently, because the initial spontaneous emission for each atom will tend to "capture" oscillations in all the other atoms The weak field induces a small polarization, as shown in Figure 2-2b, which increases the field, which in turn increases the polarization, and so on After a delay time a large and almost total polarization will result, and an emission pulse, similar to the superradiant pulse, will emerge from the system, as shown in Figure 2-2c. The system will have a rate of radiative power emission proportional to the square of the macroscopic dipole, $(N\mu_1)^2$, with a pulse width and delay time proportional to the inverse of the number of atoms (N^{-1}) There will be small random fluctuations in the delay time between initial preparation of the atoms and emergence of the superradiant pulse, because the coherent emission builds up initially from normal spontaneous emission.

A summary of the conditions and characteristics for Dicke superradiance and incoherently prepared superradiance are presented in Table 2-1 and Table 2-2, respectively.

Optical Extensions of Dicke Superradiance

The condition of a small volume V, such that V is smaller that the emission wavelength cubed ($V \leq \lambda^3$), has practically no meaning and has not been demonstrated at optical wavelengths The main reason is because there seems to be no available

Table 2.1. Summary of initial conditions and characteristics of Dicke superradiance

Type of condition	Macroscopic Polarization	Intensity Dependence	Pulse Duration	Pulse Delay	Volume of medium
Initial	$N\mu_1$	-	-	-	$V \leq \lambda^3$
$t > 0$	$N\mu_1$	$\propto (N\mu_1)^2$	$\propto N^{-1}$	-	-

N – Number of atoms

μ_1 = Dipole moment of a single atom

t = time

Table 2-2. Summary of initial conditions and charateristics for incoherently prepared Dicke superradiance.

Types of conditions	Macroscopic Polarization	Intensity Dependence	Pulse Duration	Pulse Delay	Volume of medium
Initial	none	-	-	-	$\leq \lambda^3$
$t > 0$	$N\mu_1$	$\propto (N\mu_1)^2$	$\propto N^{-1}$	$\propto N^{-1}$	-

N = Number of atoms

μ_1 = Dipole moment of a single atom

t = time

atomic medium in which a suitable number of atoms can be assembled within the small volume ($V \leq \lambda^3$) required.

A more general situation is the case where a large number of atoms, with strong inversion population, with no initial coherent polarization, are prepared in an extended region of space having a Fresnel number on the order of one. The Fresnel number is given by

$$N_f = \frac{r^2}{L\lambda} \tag{2-2}$$

where r is the radius of the cross section of this region (m), and L is the length (m). This space region is often in the form of a long cylindrical region or a pencil like region. This larger inverted region can emit either amplified spontaneous emission or a kind of Dicke superradiance known as superfluorescence, as shown in Figure 2-3, depending on the size of the inversion.

Superfluorescence

Several theories and experiments have been developed for the description of superfluorescence (40, 43-45). Superfluorescence will occur in a system under specialized conditions in which the atomic transition is strong and narrow enough, and the inversion density large enough so that the radiative coupling between atoms becomes very strong. This is similar to superradiance conditions, but in this case the atoms are spread over a larger volume. The key condition seems to be that the gain coefficient, α, must be large and the sample length small compared to the distance that radiation can

Figure 2-3 Figure showing the different steps for superfluorescence a) spontaneous emission b) the spontaneous emission induced a dipole creating some polarization of medium c) superradiant pulse

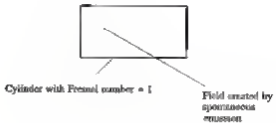
Cylinder with Fresnel number = 1
Field created by spontaneous emission

a

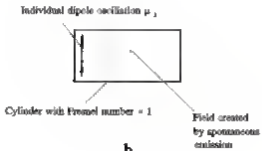
Individual dipole oscillation $\mu_{\perp}$
Cylinder with Fresnel number = 1
Field created by spontaneous emission

b

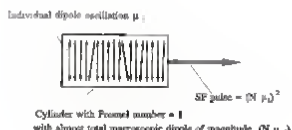
Individual dipole oscillation $\mu_{\perp}$
SF pulse = $(N\ \mu_{\perp})^2$
Cylinder with Fresnel number = 1
with almost total macroscopic dipole of magnitude $(N\ \mu_{\perp})$

c

travel in one atomic dephasing time (40). The gain coefficient is given by:

$$\alpha = \frac{3}{8}\frac{\gamma}{\gamma_a} n\lambda^2 \tag{2-3}$$

where γ is the purely radiative decay rate (s^{-1}), **n** is the number density (m^{-3}), and λ is the wavelength of the transition (m).

The conditions for superfluorescence are summarized in the following equation:

$$L_T << L << L_c \tag{2-4}$$

where L_T is, the threshold length (m), which is proportional to $1/\alpha$, where α is the gain coefficient defined in equation (2-3). L is the length of the active volume, and L_c is the cooperation length by Arecchi and Courtens (46) given by:

$$L_c = \left(\frac{8}{3}\frac{c}{n\gamma\lambda^2}\right)^{1/2} \tag{2-5}$$

where c is the speed of light ($m\ s^{-1}$).

The left hand side of the equation 2-5, is equivalent to the condition:

$$\tau_R << T_2^* \tag{2-6}$$

where τ_R is the time duration of the superfluorescence pulse (s), and T_2^* is the reciprocal of the inhomogeneous linewidth (s). This condition means that, the time scale of the cooperative emission must be shorter than the atomic relaxation times. It also means that the parameter $C >> 1$ and equivalent to the high gain condition $\alpha L >> 1$. In the case that this condition is not satisfied, the atomic decay processes would destroy cooperative emission.

In order to have superfluorescence, the cooperative emission processes must dominate the stimulated processes. The atomic medium lenght must be shorter than the cooperation length, as defined by the right-hand side of equation 2-4

Superfluorescence will be a quasi-coherent pulse of radiation, with intensity proportional to the square of the initial number of atoms, **N**. The pulse duration, and the pulse delay time will be inversely proportional to the number of atoms. Due to the nature of the initiation of the superfluorescence process, random spontaneous emission, there will be small random variations in the delay time of the pulse from shot to shot

A summary of the initial conditions and the characteristics of superfluorescence is presented on Table 2-3

Amplified Spontaneous Emission

Introduction

Amplified spontaneous emission (ASE) is the most common form of an amplifying process (40). For high-gain systems, an important phenomenon is that the amplifier can amplify not only the input field from a laser oscillator but also the spontaneous radiation emitted by the excited medium of the amplifier itself; this is also known as a mirrorless laser. This process is detrimental to stimulated emission processes ocurring in a laser amplifier

This ASE occurs when the spontaneous emission coming from a distribution of inverted atoms is amplified by the same group of atoms, but the kinds of pulse delays and large coherent polarizations that are characteristic of superradiance or

Table 2-3 Summary of initial conditions and characteristics for superfluorescence.

Type of condition	Macroscopic Polarization	Intensity Dependence	Pulse Duration	Pulse Delay	Volume of medium
Initial	-	-	-	-	cylinder shape*
$t > 0$	$N\mu_1$	$\propto (N\mu_1)$	$\propto N^{-1}$	$\propto N^{-1}$	

N = Number of atoms

μ_1 = Dipole moment of a single atom

t = time

* Cylindrical region with Fresnel number $\approx$ unity

$$N_F = r^2 / L\lambda$$

where r is the radius of the cylinder, L is the length, and λ is the transition wavelength

superfluorescence and the dependence of peak pulse intensity on N^2 do not appear in ASE. If the amplification is enough, ASE can produce a beam from the inverted medium that can be quite bright, powerful, moderately directional, with a fair amount of spatial coherence.

Allen and Peters (46-51) and several other authors (52-55) have developed and discussed different aspects of ASE theory. Allen and Peters (46) derived the threshold inversion condition for ASE, which is given by

$$n_{ab} = \frac{4\pi\tau_{21}}{\lambda^2 L}\left(\frac{\pi^{1/2}\Delta\nu_D}{2(\ln(2))^{1/2}}\right) \tag{2-7}$$

where τ_{21} is the spontaneous lifetime of the transition (s), $\Delta\nu_D$ the Doppler linewidth (s^{-1}), and L is the medium length (m).

Figure 2-4 is a pictorial representation of an amplifier medium. A very simple quantitative description of the amplifier intensity is given by a steady state equation for the propagation of intensity in an amplifying medium characterized by the gain coefficient g.

$$\frac{dI}{dz} = gI \tag{2-8}$$

If $I(0) = 0$, then $I(z) = 0$ for all z, and so equation 2-8 does not account for spontaneous emission (SE). To include SE in equation 2-8 a second term is added.

$$\frac{dI}{dz} = gI + (A_{21}nh\nu)\left(\frac{\Omega}{4\pi}\right) \tag{2-9}$$

Figure 2–4 Representation of an amplified spontaneous emission medium

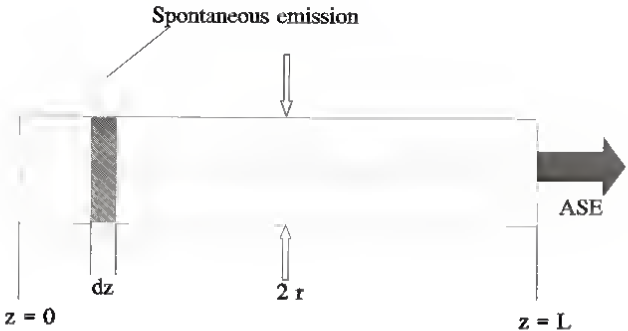
Spontaneous emission
ASE
dz
2 r
z = 0
z = L

The new added term accounts for the contribution to dI/dz from spontaneous emission of photons with energy $h\nu$ (J) by n excited atoms per unit volume (m^{-3}) with spontaneous emission rate A_{21} (s^{-1}), and $\Omega/4\pi$ is the solid angle. The right hand side of the SE term accounts for the appropriate solid angle, Ω, which is approximately equal to S / L^2, where S is the cross-sectional area of the amplifier (m^2) and L is the length (m). Integratin g dI arriving at the output end from any small dz near the input end, over the entire length L gives the expression for I (J m^{-2} s^{-1}).

$$I=\frac{nA_{21}h\nu S}{4\pi L^2}e^{gL}\int e^{gz} \tag{2-10}$$

where $n = n_2-n_1 \approx n_2$; n_1 and n_2 are the number densities (m^{-3}) of level one and two respectively. Solving equation 2-10 gives

$$I=\frac{A_{21}h\nu Sn}{4\pi gL^2}(e^{gL}-1) \tag{2-11}$$

Under saturation conditions n is given by

$$n=\frac{g_2}{g_1+g_2}n_T \tag{2-12}$$

where n_T is the total number density (m^{-3}), and g_i's are the statistical weights of the states. Substituting equation 2-12 into equation 2-11 gives.

$$I=(\frac{A_{21}h\nu S}{4\pi L^2})(\frac{g_2}{g_1+g_2})(\frac{n_T}{g})(e^{gL}-1) \tag{2-13}$$

If a large gain is assumed, $gL >> 1$, and $g = n_T \sigma$, where σ is the cross sectional area (m^2), equation 2-13 is simplified to

$$I=\left(\frac{A_{21}h\nu S}{4\pi L^2}\right)\left(\frac{g_2}{g_1+g_2}\right)\frac{e^{\sigma n_T L}}{g} \tag{2-14}$$

If a small gain is assumed, $gL << 1$, and $g = n_T \sigma$, equation 2-13 is simplified to:

$$I\propto\left(\frac{A_{21}h\nu S}{4\pi L^2}\right)\left(\frac{g_2}{g_1+g_2}\right)n_T L \tag{2-15}$$

In between these two conditions and expanding the e^{gL} term, it can be shown that $I \propto n_T^2$.

For a homogeneously broadened transition having a Lorentzian lineshape of width $\Delta\nu_L$ (s^{-1}), the cross section σ (m^2) is given by

$$\sigma=\left(\frac{\lambda^2 A_{21}}{8\pi}\right)\left(\frac{2}{\pi\Delta\nu_L}\right)=\frac{\lambda^4 A_{21}}{4\pi^2 c\Delta\lambda_L} \tag{2-16}$$

substituting σ from equation 2-16, $g = n_T \sigma$, and $\nu = c / \lambda$, in the first term of equation 2-13, and assuming high gain conditions, gives:

$$I\approx\left(\frac{\pi hc^2 S}{\lambda^5}\right)\left(\frac{g_2}{g_1+g_2}\right)\Delta\lambda_L e^{gL} \tag{2-17}$$

Saturation

Under high gain conditions ASE coming from one end of the gain medium tends to saturate the inversion over a sizable region at the opposite end of the medium. The ratio of the ASE intensity to the saturation intensity in a simple homogeneous gain medium can be expressed as

$$\frac{I}{I_{sat}} \approx \left(\frac{r}{2L}\right)^2 \left(\frac{\tau_2}{\tau_{rad}}\right) e^{\sigma n L} \qquad (2\text{-}15)$$

where r is the radius of the cross sectional area of the medium (m), and τ_2 is the effective lifetime of the transition (s), and τ_{rad} is the radiative lifetime (s).

Temporal and Spatial Output

The temporal output from ASE, consists of narrowband, highly amplified but still essentially random gaussian noise, rather than any kind of coherent or amplitude limited sinusoidal oscillation ASE, thus generally lacks most of the important temporal coherence features of a true laser oscillator

The spatial pattern from an ASE medium will be a narrow cone with a cone angle defined by the aspect ratio of the medium rod with a half angle $\Delta\theta \approx r/L$. If the rod is slender, the output can have a large degree of coherence

Cooperative Processes in Mercury

The behavior of mercury in optically pumped mixtures with nitrogen, has been studied since 1925, when Wood discovered the enhancement of the green fluorescence

of mercury in the presence of nitrogen (56). In 1974, Djeu and Burnham demonstrated and described what they called an optically pumped mercury laser (57). They pumped a mixture of mercury and nitrogen, in a slender quartz tube, with an electrodeless lamp using the scheme presented in Figure 2.5. The first excitation step in the scheme was an excitation at 253.7 nm from level 6^1S_0 to 6^3P_1, followed by a collisional deactivation of this excited state to the 6^3P_0 level. From this level, they excited with 404.7 nm to the 7^3S_1 level. An inversion of population was created between the 7^3S_1 and the 6^3P_2 level, creating the conditions to have ASE. In 1978, Holmes and Siegman, using the same pumping scheme, studied in more detail the mercury-nitrogen laser (58).

Figure 2-5 Mercury partial energy levels diagram showing pumping scheme used by Djeu for the optically pumped mercury-nitrogen laser

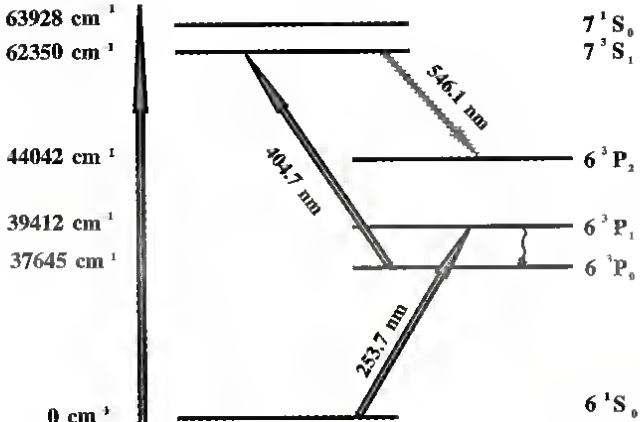
63928 cm⁻¹
62350 cm⁻¹
44042 cm⁻¹
39412 cm⁻¹
37645 cm⁻¹
0 cm⁻¹
7 ¹S₀
7 ³S₁
6 ³P₂
6 ³P₁
6 ³P₀
6 ¹S₀
546.1 nm
404.7 nm
253.7 nm

CHAPTER 3
RATE EQUATIONS APPROACH

Introduction

As discussed in chapter one, the energy density of a laser is high enough to greatly enhance the population of the excited state when compared with the thermal population existing before the laser pulse. If the energy is less than that needed to obtain saturation, the populations of the levels will be controlled by the Einstein coefficient of spontaneous emission and the collisional deactivation rates. If the energy is high enough, the transition can be saturated and the population of the two levels involved will be locked together in the ratio of their respective degeneracies. This laser field is considered to be a quasicontinuum, because the spectral width exceeds the width of the atomic absorption profile (14,24). The excited atoms can undergo several pathways, such as radiative deactivation, collisional deactivation, collisional excitation, and chemical reactions.

To be able to describe and predict the behavior of the populations of the different levels, and some parameters from the atomic fluorescence system, a theoretical or mathematical approach is needed. Although an accurate description of this type of system is given by the tedious and complicated density matrix equations, several authors have used the less complicated rate equation formulation with good results (59-64). In

this chapter the considerations and assumptions of the rate equations approach are pointed, a simple example on how to solve the rate equations is given, and then the rate equations are set for the studied mercury system.

Theoretical Considerations

There are several considerations and assumptions that are made in order for the rate equations to be valid. First, the laser is assumed to be a spectral continuum when compared with the atomic absorption profile, which avoids consideration of coherence effects. The laser beam is also assumed to be spatially homogeneous. The temporal behavior of the laser is assumed to have a rectangular shape, with duration Δt_i (s), and because short laser pulses (less than ten nanoseconds) are considered, the possibility of having chemical reactions, or recombination of ions and electrons, is not considered.

In Figure 3-1, a three level system is presented. The following rate equations analysis is the same as the one presented by Omenetto, Smith and Hart, in their treatment of ionization spectroscopy (63) but here level 1 is level three here. In the system presented, by Omenetto, et al. (63), only one laser is present and it is tuned to λ_{12}, collisions are the only way excited atoms in level two are transferred to level three. The number densities (m^{-3}) of levels one, two, and three are given by n_1, n_2, and n_3 respectively. The total atomic population is given by n_T (m^{-3}),

$$n_T = n_1 + n_2 + n_3 \tag{3-1}$$

The rate equations for the system are given by:

Figure 3-1 Energy levels diagram of the system used in the text Refer to text for explanation of the symbols used

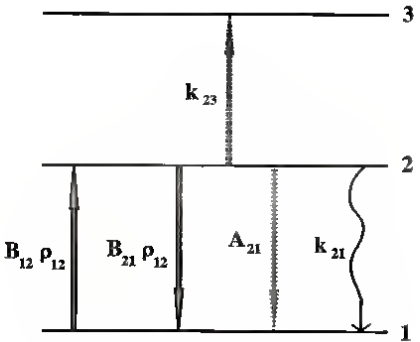
3
k 23
2
B12 ρ12
B21 ρ12
A21
k 21
1

$$\frac{dn_3}{dt} = R_{23} n_2 \tag{3-2}$$

$$\frac{dn_2}{dt} = R_{12} n_1 - n_2 (R_{23} + R_{21}) \tag{3-3}$$

where $R_{12} = B_{12}\,\rho_{12} + k_{12}$, $R_{23} = k_{23}$, $R_{21} = A_{21} + k_{21} + B_{21}\,\rho_{12}$, ($s^{-1}$). The collision deexcitation coefficients (s^{-1}), are given by the k_{ij}'s, the Einstein coefficient of spontaneous emission (s^{-1}) by A_{21}, the Einstein coefficient of stimulated absorption and emission ($m^4\,s^{-1}\,J^{-1}$), are given by B_{12} and B_{21} respectively, and the laser spectral energy density ($J\,m^{-4}$) is given by ρ_{12}. The spectral energy density is give by

$$\rho_{12} = \frac{E_{12}}{\Delta t_l S \Delta \lambda_l c} \tag{3-4}$$

where E_{12} is the laser energy (J), λ_{12} is the transition wavelength (m), S is the cross sectional area of the laser beam (m^2), Δ_l is the laser linewidth (m), and c is the speed of light ($m\,s^{-1}$)

Using standard methods for the solution of differential equations, with D being the differential operator, and expressing n_1 in terms of n_T, we get

$$(D + R_{12} + R_{23} + R_{21})\, n_2 = R_{12}\, n_T - R_{12}\, n_3 \tag{3-5}$$

$$\frac{Dn_3}{R_{23}} = n_2 \tag{3-6}$$

$$n_3[D^2 + D(R_{12} + R_{23} + R_{21}) + R_{12} R_{23}] = R_{12} R_{23}\, n_T \tag{3-7}$$

Solving the quadratic equation in D gives

$$D = \frac{-X \pm \sqrt{X^2 - 4Y}}{2} \tag{3-8}$$

where $X = R_{12} + R_{21} + R_{23}$, and $Y = R_{12} R_{21}$.

The general solution for $n_3(t)$ is given by

$$n_3(t) = C_1 e^{-\alpha_2 t} + C_2 e^{-\alpha_3 t} + C_0 \tag{3-9}$$

where C_1, C_2, and C_0 are the integration constants and the α's are given by

$$\alpha_2 = \frac{X - \sqrt{X^2 - 4Y}}{2} \tag{3-10}$$

$$\alpha_3 = \frac{X + \sqrt{X^2 - 4Y}}{2} \tag{3-11}$$

An expression for $n_2(t)$ can also be derived, and it is given by:

$$n_2(t) = -\frac{1}{R_{23}}(\alpha_2 C_1 e^{-\alpha_2 t} + \alpha_3 C_2 e^{-\alpha_3 t}) \tag{3-12}$$

Having the initial conditions of $n_3(t) = n_2(t) = 0$ at time $t=0$, results in $C_1 + C_2 = -C_0$, and solving for the C's results as follows:

$$C_1 = C_0 \frac{\alpha_3}{\alpha_2 - \alpha_3} \tag{3-13}$$

$$C_2 = C_0 \frac{\alpha_2}{\alpha_2 - \alpha_3} \tag{3-14}$$

$$C_0 = n_T \tag{3-15}$$

The result for C_0 is the steady-state value when $t = \infty$ and $D = 0$. The final expressions for the time dependents n_1 and n_2 are given by

$$n_3(t) = n_T\left(1 + \frac{\alpha_3}{\alpha_2 - \alpha_3} e^{-\alpha_2 t} - \frac{\alpha_2}{\alpha_2 - \alpha_3} e^{-\alpha_3 t}\right) \tag{3-16}$$

$$n_2(t) = n_T \frac{\alpha_2 \alpha_3}{R_{23}(\alpha_2 - \alpha_3)}\left(e^{-\alpha_3 t} - e^{-\alpha_2 t}\right) \tag{3-17}$$

For systems with more levels, solving the equations can get more complicated and time consuming, so that solving them numerically using a computer is preferred.

Mercury Rate Equations

In Figure 3-2, the different excitation and deexcitation processes, with their respective rates, are presented for mercury. The rate equations can be set as follows:

$$\frac{dn_2}{dt} = r_{20} n_2 + r_{10} n_1 - r_{02} n_0 \tag{3-18}$$

$$\frac{dn_1}{dt} = r_{41} n_4 + r_{21} n_2 - (r_{10} + r_{12}) n_1 \tag{3-19}$$

Figure 3-2 Partial energy diagram of mercury showing the different excitation and deexcitation processes

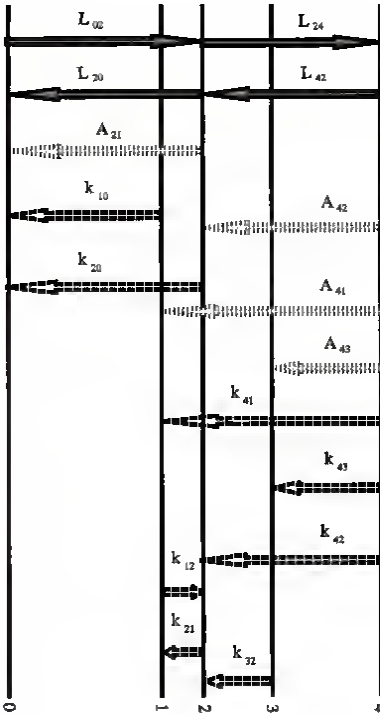
L 02
L 20
A 21
k 10
k 20
k 12
k 21
L 24
L 42
A 42
A 41
A 43
k 41
k 43
k 42
k 32
0
1
2
3
4

$$\frac{dn_2}{dt}=r_{02}n_0+r_{42}n_4+r_{32}n_3+r_{12}n_1-(r_{21}+r_{24})n_2 \tag{3-20}$$

$$\frac{dn_3}{dt}=r_{43}n_4-r_{32}n_3 \tag{3-21}$$

$$\frac{dn_4}{dt}=r_{24}n_2-(r_{42}+r_{41}+r_{43})n_4 \tag{3-22}$$

where the total rates (s^{-1}), r_{ij}'s are given by:

$$r_{20}=L_{20} \tag{3-24}$$

$$r_{10}=k_{10} \tag{3-25}$$

$$r_{41}=A_{41}+k_{41} \tag{3-26}$$

$$r_{21}=k_{21} \tag{3-27}$$

$$r_{12}=k_{12} \tag{3-28}$$

$$r_{42}=L_{42}+A_{42}+k_{42} \tag{3-29}$$

$$r_{32}=k_{32} \tag{3-30}$$

$$r_{24}=L_{24} \tag{3-31}$$

$$r_{43}=A_{43}+k_{43} \tag{3-32}$$

In this case, L_{02} and L_{20}, L_{24} and L_{42}, are the product of the Einstein coefficient of stimulated absorption, and stimulated emission, for the first and second transition respectively.

The Einstein coefficient of stimulated absorption ($m^4\ s^{-1}\ J^{-1}$), is given by

$$B_{ij} = \frac{10^7 A_{ji} g_j \lambda^5}{8\pi h g_i c} \tag{3-18}$$

where A_{ji} is the Einstein coefficient of spontaneous emission (s^{-1}), g_i and g_j are the statistical weights of the states, λ is the transition wavelength (m), h is Plank's constant (J s), and c is the speed of light (m s^{-1})

The spectral energy density ρ_{ij} (J m^{-4}), is given by equation 3-4 In Table 3-1, a list of the different values of parameters used is presented Using these parameters the following calculations can be made, for the first laser excitation, with energy of 1 μJ and diameter of 3 mm

$$B_{02} = \frac{10^7 (1.3\times10^{3})(4)(253.7\times10^{-9})^5}{8\pi(6.6\times10^{-34})(1)(3\times10^{8})}$$

$$\approx 1.1 \times 10^{5}\ m^4\ s^{-1}\ J^{-1}$$

$$\rho_{02} = \frac{(1\times10^{-6})}{(10^{-9})(\pi(3\times10^{-3})^2)(30\times10^{-12})(3\times10^{10})}$$

$$\approx 3.9 \times 10^{8}\ J\ m^{-4}$$

for the second laser excitation, with an energy of 1 μJ and diameter of 4 mm

Table 3-1 List of parameters used for the development of the rate equations for mercury

Transition Wavelength (nm)	i	j	A_{ij}* $10^7(s^{-1})$	k_{ij} $10^3(s^{-1})$	g_i	g_j	B_{ij}† 10^5 $(m^4 s^{-1} J^{-1})$	B_{ji}‡ 10^5 $(m^4 s^{-1} J^{-1})$
253.7	0	2	1.3 ± 50%	0.00630 ± 3%	1	4	1.1	0.28
435.8	2	4	4.0 ± 50%	1.0 ± 50%	2	3	9.4	6.3
546.1	3	4	5.6 ± 50%	7.0[a,b] ± 50%	5	3	-	-
404.7	1	4	1.7 ± 50%	1.0 ± 50%	1	3	-	-
-	0	1	-	0.18 ± 50%	1	1	-	-
-	1	2	-	1.14 ± 10%	1	4	-	-
-	2	1	-	0.00067 ± 10%	4	1	-	-
-	2	3	-	30[a,b] ± 35%	4	5	-	-

* From reference 39

** From reference 58

† Refer to text for calculation and conditions

‡ Note that $B_{ji} = B_{ij}(g_i / g_j)$

[a] From reference 57

[b] Units are in $(s^{-1} torr^{-1})$ for nitrogen as buffer gas

$$B_{24} = \frac{10^7(4.0\times10^7)(3)(435.8\times10^{-9})^5}{8\pi(6.6\times10^{-34})(4)(3\times10^{10})}$$

$$= 9.4 \times 10^5 \ m^4 \ s^{-1} \ J^{-1}$$

$$\rho_{24} = \frac{(1\times10^{-6})}{(10^{-8})(\pi(4.0\times10^{-3})^2)(30\times10^{-12})(3\times10^8)}$$

$$\approx 2.2 \times 10^8 \ J \ m^{-4}$$

Note that the Einstien coefficient of stimulated emission ($m^4 \ s^{-1} \ J^{-1}$), $B_{ij} = B_{ji} \ (g_i / g_j)$

These equations can be used for the description of the population distribution of the double resonance excitation mercury fluorescence system in Figure 3-2. For a complex equation system like this, a numerical solution is performed using a computer. The program used for the solution of these equations is presented in appendix A

CHAPTER 4
EXPERIMENTAL

Laser Excited Atomic Fluorescence Spectrometry

Instrumentation and Operational Parameters

The schematic diagram of the optical layout is shown in Figure 4-1 and is similar to the one used by Vera et al (9). A XeCl excimer laser (Lumonics TE 860-4, Lumonics, Ontario, Canada) was used to pump two dye lasers (Molectron DL-14, Laser Photonics, Orlando, FL) at a frequency of 10 Hz. The dye lasers which where aligned spatially and temporally, used Coumarin 500 and Coumarin 440 (Exciton 05000 and 04400, Dayton, OH). The laser energies were measured with a calibrated pyroelectric Joulemeter (Model J3-09C, Molectron Detector, Incorporated, Portland, OR). The Joulemeter was calibrated for termination on 50 Ω resistor, and its output was a voltage, monitored in an oscilloscope, with the peak amplitude of this voltage proportional to the energy of the laser pulse. The fundamental of one dye laser at 507 nm was frequency doubled with a BBO crystal with an output energy of 60 μJ at 253.7 nm. The output energy of the other dye laser at 435.8 nm was 90 μJ. The lasers energies were monitotud during the experiments to ensure optical saturation conditions. Laser tuning was performed by using a Hg vapor cell and measuring fluorescence using the forst surface configuration

Figure 4-1 Schematic diagram of the optical layout. The furnace and the mercury cell can be interchangeably placed in the optical path

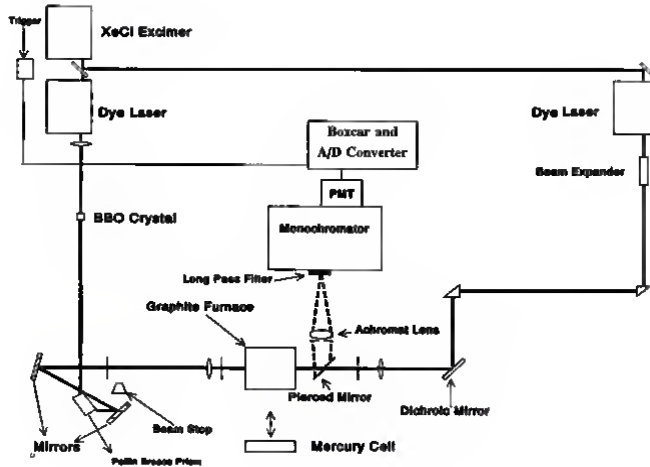
Trigger
XeCl Excimer
Dye Laser
Boxcar and
A/D Converter
Dye Laser
Beam Expander
PMT
BBO Crystal
Monochromator
Long Pass Filter
Graphite Furnace
Achromat Lens
Pierced Mirror
Dichroic Mirror
Beam Stop
Mirrors
Pellin Broca Prism
Mercury Cell

The furnace (Perkin-Elmer HGA-400, Perkin-Elmer, Norwalk, CT) was placed on a platform to allow translation perpendicular to the optical axis as shown in Figure 4-1. The furnace window mounts were tilted so the windows were at an angle to the excitation beam to minimize collection of the reflected laser radiation by the monochromator. Pyrocoated graphite tubes equipped with a L'vov platforms were used for the furnace.

The fluorescence was collected with an achromat lens (focal length = 10 cm, *f/#* 2), and detected with a double monochromator (focal length = 22 cm , *f/#*4, SPEX 1680, 500 nm blazed gratings, SPEX, Edison, NJ) with a slit width of 1 mm and a PMT (Hamamatsu 1P28, Hamamatsu, Bridgewater, NJ). An achromat lens was used to image the fluorescence on the monochromator entrance slit, the achromatic lens resulted in the best signal-to-noise ratio (8). An aperture was used in front of the lens in order to match the *f/#* of the collection optic with the monochromator *f/#* (where the lens *f/#* = focal length / diameter).

A long pass filter (Hoya Y-52, Hoya Optics Incorporated, Sturbridge, Mass.) was used in front of the entrance slit, to lower the laser scatter. When necessary, and to avoid saturation of the PMT, neutral density filters (ORIEL Corporation, Stratford, CT) were used in front of the entrance slit, to attenuate the intensity of the fluorescence. The optical density, D, of a given filter is defined as

$$D = \log_{10}\frac{I_0}{I_T} \tag{4-1}$$

where I_0 is the incident power (W) and I_T is the transmitted power (W). The transmittance of a filter can be calculated as:

$$T = 10^{-D} \tag{4-2}$$

Since the optical densities of the filters are additive, several filters can be used to produce higher attenuation of the fluorescence. The optical density in that case will be given by

$$D_{Total} = \sum D_i \tag{4-3}$$

where D_i is the optical density of one filter.

The PMT was terminated in a 1200 Ω load resistor and the signal processed by a boxcar (Stanford SR250, Stanford Research, Palo Alto, CA) and an analog-to-digital interface (Stanford SR245, Stanford Research, Palo Alto, CA), and collected by computer. A boxcar time constant of 1 s was used for all measurements. The electronic detection system was triggered by a fast photodiode triggered by the excimer laser.

Mercury solutions were prepared using a 1000 part per million (ppm) mercury standard (SPEX, Edison, NJ) and low conductivity de-ionized water. Injections of 10 μL aliquots were introduced into the furnace using a micropipette (Eppendorf Comforpette 4700, Eppendorf, Madison, WI).

In Figure 4-2, the two-step excitation scheme with the corresponding fluorescence emission lines is shown. The scheme used a first excitation at λ_1 = 253.7 nm and a second excitation at λ_2 = 435.8 nm. Fluorescence was observed at λ_{01} = 546.1 nm, λ_{02} =

Figure 4-2. Partial energy diagram for mercury.

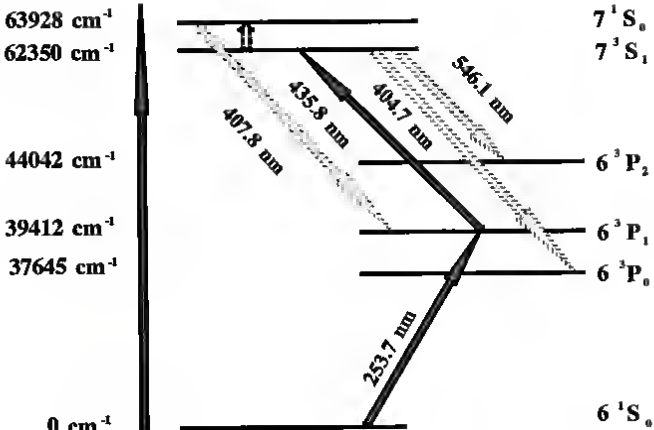
63928 cm-1
62350 cm-1
44042 cm-1
39412 cm-1
37645 cm-1
0 cm-1
7 1S0
7 3S1
6 3P2
6 3P1
6 3P0
6 1S0
407.8 nm
435.8 nm
404.7 nm
546.1 nm
253.7 nm

404 7 nm, or at λ_m= 407 8 nm As can be seen, two of these lines are optically coupled and the third at 407 8 nm is populated by collisions

Elimination of Mercury Loss

Because of the volatility of mercury, loss during the drying step in the furnace was a major problem Grobenski, et al (36) showed that the problem of mercury loss can be solved by matrix modification.

The furnace temperature program used before finding this literature was for step one, the drying step, a 110 °C temperature was maintained for 40 s, and as a second step atomization at a temperature 1100 °C was maintained for 5 s The atomization step was performed under stopped flow conditions

The furnace temperature program was modified to follow the suggestions of Grobenski et al (36) Palladium was added as a matrix modifier to avoid loss of mercury during the drying step The palladium 1000 ppm stock solution (SPEX, Edison, NJ) was used directly, injections of 20 μL aliquots were introduced into the furnace using a micropipette (Eppendorf, Madison, WI). After injecting the palladium solution, the program was started, with a ramp of 5 s from 25 °C to 110°C, which was maintained for 35 s An atomization step was performed at 1200° C for 5 s After that, a room temperature step allowed time to inject the 10 μL of 100 ppb Hg solution The drying and atomization steps times and temperatures were the same as those used for palladium, but the atomization step was performed under stopped flow conditions A cleaning step

at 2000 °C ended the program. This modified program is shown schematically in Figure 4-3.

Determination of the Instrumental Limit of Detection

The instrumental limit of detection (LOD) was determined for the fluorescence at λ_{III} and λ_{III}. The instruments, parameters and furnace temperature program mentioned above were used for the determination of the LOD. It is important to note that the long pass filter was removed for the determination at λ_{III} because the cut off wavelength was ≈ 510 nm. All measurements were performed using a mercury solution of 100 ppb, and they were in triplicate. The LOD is defined by the following equation:

$$LOD = k(C_a)(\frac{N}{S}) \qquad (4\text{-}4)$$

where S is the signal in V-s, N is the Noise in V-s, C_a is the analyte concentration, and k is the confidence factor (chosen to be 3).

The signal were measured as the sum of the signals of the each point in the peak, which is proportional to the area of the peak. The noise were taken by letting the lasers running over a period of time, without running the furnace, assuming that the only source of noise was from the scatter of the lasers. A calculation of the average of the signal peak width was done. This peak width (PW_i) was used to calculate the noise as follows: 1) a section in the plot of signal versus time of width equal to $3PW_i$ was randomly selected, 2) the average of the average signals for the first and last section of width PW_i was subtracted as the background, 3) the area of the central section was calculated, 4)

Figure 4-3 Graphite furnace temperature program

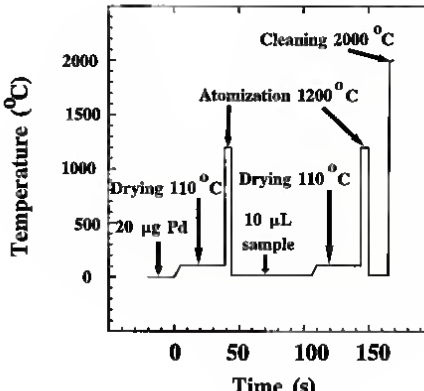
Cleaning 2000 °C
Atomization 1200 °C
Drying 110 °C
Drying 110 °C
20 µg Pd
10 µL
sample
Temperature (°C)
2000
1500
1000
500
0
0
50
100
150
Time (s)

the first 3 steps were repeated several times 5) the standard deviation of the areas calculated in step 3 was taken as the noise This way of calculating the noise is a tedious and a time consuming process, and so a computer program was developed to perform the calculation (see appendix B) To compare if there was a significant difference between the calculation performed manually and the one performed by the computer, a student t-test was carried out (65)

Calibration Curves

The calibration curves for λ_{III} and λ_{III} were obtained The instrumentation parameters were mentioned in a preceding section Triplicate measurements were done for the blank, and mercury solutions at 0 01, 0 02, 0 04, 0 06, 0 08, 0 1, 0 2, and 1 0 part-per-million (ppm) for the calibration curve at λ_{III} For λ_{III}, the measurements started with mercury solutions of 0 1, 0.2, 1, 10, and 100 ppm

Amplified Spontaneous Emission

Instrumentation and Operational Parameters

The schematic diagram of the optical layout for amplified spontaneous emission (ASE) is shown in Figure 4-4 The main components and parameters are the same as the ones presented in the LEAFS-ETA section For this case in particular, the atom reservoir was a vapor cell (Glass Shop, Department of Chemistry, University of Florida), instead of the graphite furnace. Also, the collection of the ASE was made at 180° with respect to the optical axis The ASE was collected with an achromat lens and focused

Figure 4-4 Schematic diagram of the optical layout for the amplified spontaneous emission experiments

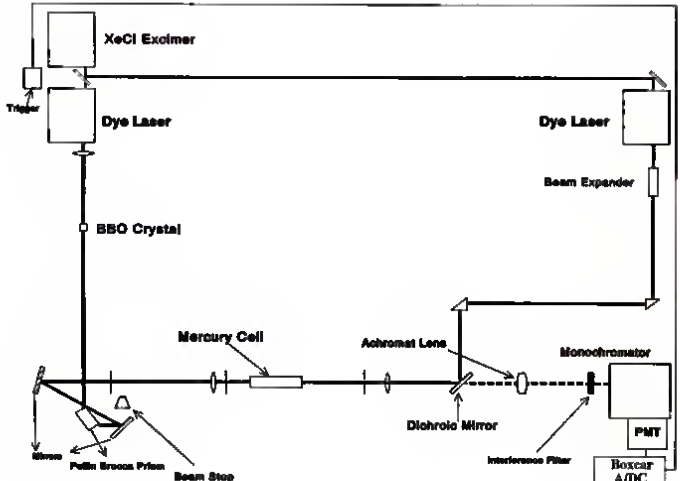
XeCl Excimer
Trigger
Dye Laser
Dye Laser
Beam Expander
BBO Crystal
Mercury Cell
Achromat Lens
Monochromator
Dichroic Mirror
PMT
Mirror
Pellin Broca Prism
Beam Stop
Interference Filter
Boxcar
A/DC

into the entrance slit of the monochromator, (H-10V American ISA, Metuchen, NJ, focal length = 10 cm, without slits) that was fitted with a PMT (R1414, Hamamatsu, Bridgewater, NJ). An interference filter (Model 54660, Oriel Corporation, Stratford, CT) was place in front of the entrance of the monochromator. Neutral density filters were also used, when necessary to attenuate the intensity of the ASE. The signal was processed, as in the LEAFS-ETA setup, by a boxcar, analog to digital interface and a collected by the computer.

Vapor Cells

Three different vapor cells were used for the ASE experiments. The first design, cell-I, which is shown in Figure 4-5, was already available in the laboratory and was routinely used for checking the alignment and tuning of the lasers. This cell (8cm x 5 cm o d) had quartz windows, that were attached by the glass shop. Several grams of mercury were placed in it with what is believed to be N_2 as buffer gas, with a pressure = 500 torr. There is no record on the procedure on how the cell was made, or the pressure of the buffer gas. The other two cells were design for the ASE experiments.

The design of the second cell-II used is presented in Figure 4-6. This glass cell had quartz windows fixed by using high vacuum epoxy. Three small drops of mercury were place in it and a teflon high vacuum stopcock (Rotaflo by Corning, Corning, NY) was used to seal it. The water jacket around it allowed for cooling or heating.

The design of the third cell-III design used is presented in Figure 4-7. This cell was also made from glass, and the quartz windows were fixed by using high vacuum

Figure 4-5. Cell design-I

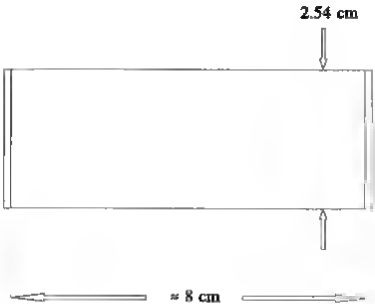
2.54 cm
≈ 8 cm

Figure 4-6. Mercury vapor cell-II, designed to allow cooling and heating.

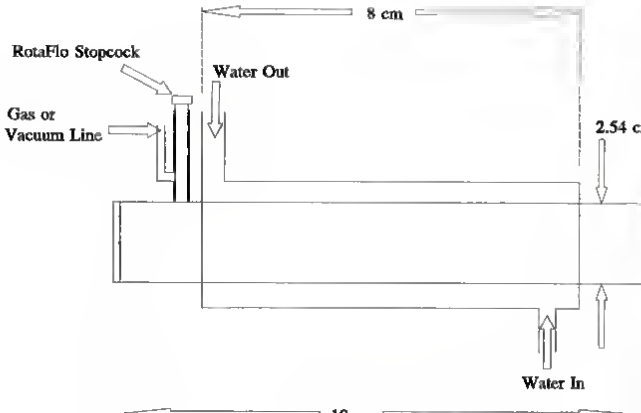
8 cm
RotaFlo Stopcock
Water Out
Gas or
Vacuum Line
2.54 cm
Water In
10 cm

Figure 4 7. Mercury vapor cell-III In this design the mercury is kept in a different compartment of the cell

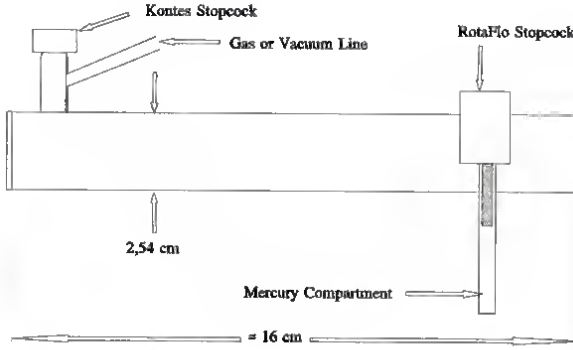
Kontes Stopcock
Gas or Vacuum Line
RotaFlo Stopcock
2,54 cm
Mercury Compartment
≈ 16 cm

epoxy A few grams of mercury were placed in a separate compartment and sealed by a high vacuum stopcock (Rotaflo by Corning, Corning, NY) By cooling the separate compartment to liquid nitrogen temperatures, this design allows pumping of the cell without letting mercury into the vacuum system The main compartment of this cell was sealed by using a high vacuum stopcock (Kontes, Kontes Glass, Vineland, NJ)

Saturation Curves

The laser beams were attenuated by placing colored glass neutral density filters (Oriel Corporation, Stratford, CT) at the exit of the respective dye laser The laser energies were measured at the point in the optical path where the cell-I was to be placed for the measurement. The measurements of the first transition saturation curve were performed at 8 8 °C to make sure that the cell was not optically thick

The background noise was measured for 20 s by running the system without the cell in the optical path The cell was, then placed in the optical path and the signal+background was measured for 20 s The signal was calculated by subtracting the average of the background measurement from the signal+background measurement.

ASE Dependence on Number Density of Mercury

Cell-II was filled with argon as buffer gas as described in the preceding section After placing the cell in the optical path, the temperature control system shown in Figure 4-8, was connected. The temperature control system consisted of two water reservoirs, the first one was a buffer reservoir filled with water and the second was the cooling or

Figure 4-8 Schematic diagram of the cooling and heating system

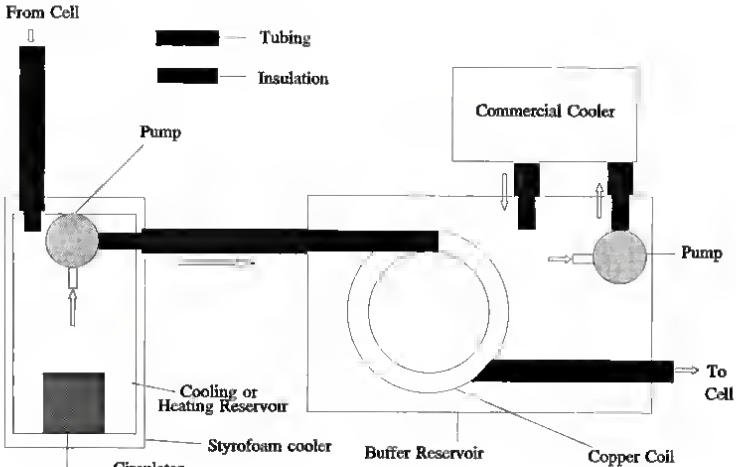
From Cell
Tubing
Insulation
Commercial Cooler
Pump
Pump
To Cell
Cooling or Heating Reservoir
Styrofoam cooler
Circulator
Buffer Reservoir
Copper Coil

heating reservoir, which was kept insulated in a styrofoam cooler When the lowest temperature (≈ 2 °C) was needed the water from the buffer reservoir was circulated by a water pump (Model CP-6500T, Little Giant, Oklahoma City, OK) to a commercial cooling system After the measurement at this temperature was obtained, the pump and the commercial cooling system were turned off The water from the cooling or heating reservoir was circulated by a water pump (Model CP-6500T, Little Giant), to a copper coil inside the buffer reservoir, and from there into the cell From the cell, the water came back to the cooling or heating reservoir For the lowest temperature (≈ 2 °C) the cooling or heating reservoir was filled with water and ice After the measurement at this temperature was obtained, some of the ice was taken out of the reservoir, and a circulator (Model 1252-00, Cole Palmer Instruments Company, Chicago, Ill) was used to heat the water gradually This cooling and heating system had a temperature stability of ≈ ± 0 1 °C

When the cell-1, a copper jacket was available to allow cooling or heating of the cell The above cooling or heating system was connected to the jacket that was placed around the cell

The number density in both cases was calculated from the vapor pressure of mercury using the following equation

$$\log p = -\frac{A}{T} + B + C\log T + DT \tag{4-4}$$

where p is the pressure in torr and T is the temperature in K The values of A, B, C, D were calculated by fitting the data from a table in reference 30 to the equation (4-4)

The values found where, A = 3339 torr K , B = 10 torr, C = -0.78 torr , and D = 6.6 x 10^{-5} torr K^{-1} The signal and noise measurements were performed as in the preceding sub-section, for each number density

A study of ASE dependence on number density was also done in the graphite furnace The signal was measured in triplicate, and the areas were measured as described in the sub section on Determination of Instrumental Limit of Detection in the LEAFS-ETA section preceding this one,

ASE Dependence on Type of Buffer Gas

The mercury vapor cell-II was evacuated to several hundred millitorr for not less than 5 min, by a mechanical pump (Type 1030, Alcatel, Hanover, Mass.) that was protected from mercury gases by a liquid nitrogen trap After closing the stopcock, a flow of the buffer gas was blow over the entrance tubing to sweep the air trapped in it. After several minutes of purging, the buffer gas line was connected, and the stopcock was opened The intensity of the ASE with, air, nitrogen, and argon, was measured as shown in Figure 4-4, and processed as discussed in the section above

The ASE dependence on type of buffer gas was studied in the graphite furnace, Triplicates of the measurement were done by injecting 10 μL aliquots of a 1 ppm mercury solution into the furnace In the first case, the normally used argon buffer, was connected to the gas line of the graphite furnace Then, the gas line was changed to the laboratory nitrogen line, and the measurement performed by using the latter as the buffer gas. Air was not used as a buffer gas, because it will destroy the graphite

ASE Dependence on Nitrogen Gas Pressure

To evacuate the cell used in this experiment, cell-III, a high vacuum system which was available in the laboratory was used. This system, shown in Figure 4-9, is capable of achieving pressures of 10^{-6} torr. The procedure on how to use the system is described by Ayala (65). To prepare the cell, the mercury compartment was cooled to liquid nitrogen temperatures, then both stopcocks (refer to Figure 4-7) were opened. After achieving $\approx 10^{-6}$ torr, the cell was left for 5 minutes. After closing the system valves and the mercury compartment in the cell, the necessary amount of nitrogen gas was added to the cell to obtain the desired pressure. The cell was placed in the optical path and measurement of the signal was performed as described in the preceding sub-sections.

Figure 4-9 Schematic diagram of vacuum system.

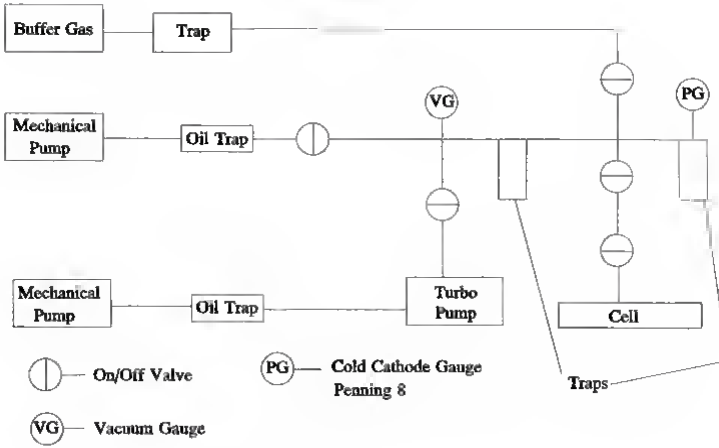
Buffer Gas
Trap
Mechanical Pump
Oil Trap
VG
PG
Mechanical Pump
Oil Trap
Turbo Pump
Cell
Traps
On/Off Valve
PG
Cold Cathode Gauge
Penning 8
VG
Vacuum Gauge

CHAPTER 5
RESULTS AND DISCUSSION

Laser Excited Atomic Fluorescence Spectrometry

Elimination of Mercury Loss

After the use of Pd as matrix modifier, and making the modifications in the graphite furnace temperature program suggested by Grobenski et al (36), the mercury loss was eliminated. Grobenski and co-workers (36) thought that the mechanism of the matrix modification was a simple amalgamation, but this was not the case because they tried gold and platinum and neither of these metalsworked. They pointed out, though, that the only difference between these three elements, was that palladium readily forms oxides which seems to be somehow required or involved in the atomization of mercury. This point was tested by using silver, which also forms oxides. Good results were obtained, suggesting that oxide formation is necessary. Rettberg and Beach (66), stated that the reaction leading to analyte stabilization occured at the surface of Pd droplets formed in the furnace. The analytical usefulness of Pd as a modifier would then be related to the ability to create a clean Pd surface and the amount of Pd surface-area exposed (66). This same argument has been established to describe the effectiveness of supported catalyst materials, including Pd catalysts (67). References can be found which

show evidence of Pd droplets formation on surfaces, where Pd catalyst were supported (68-69).

In Figures 5-1 and 5-2 the difference between not using the matrix modifier, and using palladium as a matrix modifier, is shown. It is worth noting that the concentration shown in Figure 5-2 is 10 times smaller than that for Figure 5-1.

Determination of Instrumental Limit of Detection

The typical signal output of the boxcar is presented in Figure 5-3. A 1.0 neutral density filter was inserted at the spectrometer for concentrations above 10 ppb in order to maintain linearity in the PMT. The limits of detection (LOD) obtained are given in Table 5-1. The LOD for the 546.1 nm fluorescence line was best. The limiting noise, regardless of the fluorescence wavelength used, was laser-induced noise due to detection of stray light at either 507.4 nm (the fundamental output of the 253.7 nm laser beam) or 435.8 nm. This level of laser-induced noise was about 2X greater than the noise level produced by radio-frequency pick up from the firing of the excimer laser and about 4X greater than the detector dark noise. A comparison of the limits of detection obtained by other techniques is given in Table 5-2. As can be seen, only two techniques allowed direct determination of mercury. Even though several of them report sub-pptr LOD's, their absolute LOD is poor compared with this work, because of the pre-concentration step. The practical detection limit was blank limited; the best available water in our laboratory contained about 1 ng/mL Hg.

Figure 5-1. LEAFS-ETA signal for mercury during the furnace program. The figure shows the mercury loss during the drying step

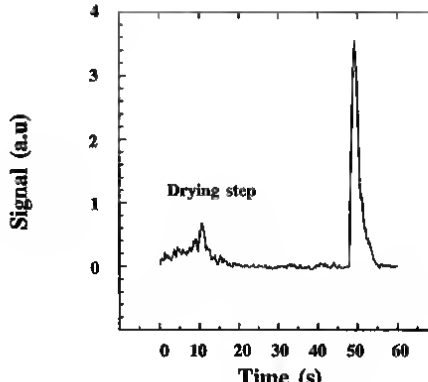
Signal (a.u)
4
3
2
1
0
Drying step
0
10
20
30
40
50
60
Time (s)

Figure 5-2 LEAFS-ETA signal for mercury, with Pd as matrix modifier, and modifications to the furnace program. This clearly shows that the problem of mercury loss during the drying step was eliminated.

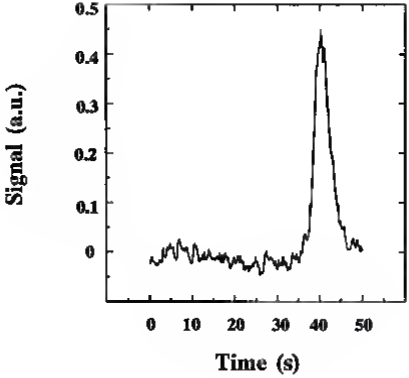
0.5
0.4
0.3
0.2
0.1
0
Signal (a.u.)
0
10
20
30
40
50
Time (s)

Figure 5-3. Typical signals of the LEAFS-ETA system for three mercury standards analyzed in duplicate. The 20 and 40 ppb signals were recorded with a 1.0 neutral density placed at the monochromator entrance slit in order to preserve PMT linearity. The abscissa has been scaled accordingly.

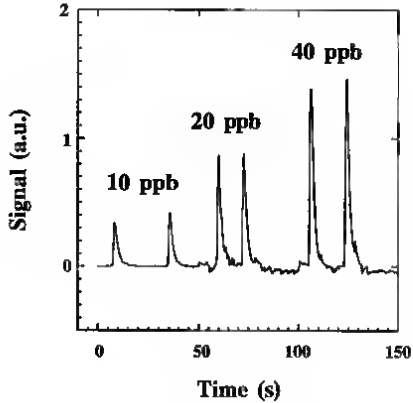
40 ppb
20 ppb
10 ppb
Signal (a.u.)
2
1
0
0
50
100
150
Time (s)

Table 5-1 Instrumental limits of detection for LEAFS-ETA determination of mercury

Fluorescence Wavelenght (nm)	LOD* pg (fg)	LOD* ppb (pptr)
546.1	10 (90**)	1 (9**)
404.6	(500**)	(50**)

* LOD = Limit of Detection

** Laser scatter limited LOD

Table 5-2 Comparison of results for mercury determination with different techniques

Method*	LOD (fg)**	LOD (pptr)**	Observations (D / P)***	Reference
AA-CV	200,000	20	P	32
DRI	337	ND	P	33
FL-CV	5000	0.1	P	34
AA-Pt-ETA	30,000	0.6	P	35
AA-ETA	25,000	500	D	36
ICP-MS	ND	30	D	37
LEAFS-ETA	10000(90†)	1000(9†)	D	This Work

* AA = Atomic absorption
CV = Cold vapor
DRI = Double resonance ionization
FL = Fluorescence
ETA = Electrothermal atomization
Pt-ETA = Platinum coated graphite tube
ICP-MS = Inductively coupled plasma mass spectrometry
LEAFS = Laser excited atomic fluorescence

** ND = Not determined

*** D = Direct
P = Pre-concentration

† Laser scatter limited LOD

All the noise measurements were performed using the program listed in Appendix B. These calculations were compared with the calculations made manually by means of a student t-test. Two conditions must be met for the validity of the t-test. The first one was the condition of the variable normally distributed in the population, which in this case was assumed. The second, the condition of homogeneity of the variances was checked by performing the F-test. The results of the Student t-test are presented in Table 5-3. From the results of the t-test for the confidence and degrees of freedom stated, it can be concluded that the standard deviations of the blanks signal calculated by the computer and the standard deviation of the blanks calculated manually are the same.

Calibration Curves

Analytical calibration curves for λ_{ni} = 546.1 nm and λ_{ni} = 407.8 nm are shown in Figure 5-4. The linear dynamic range (LDR) at λ_{ni} = 546.1 nm is limited at high concentrations where amplified spontaneous emission ASE occurs and a collimated beam of stimulated fluorescence emerges from the graphite furnace collinear with the lasers. The effect of ASE in the calibration curve at λ_{ni} = 546.1 nm is shown in Figure 5-5. However, the ASE was spatially filtered to some extent by the pierced mirror which allowed most of the atomic fluorescence to be detected while most of the ASE passed through the hole on the pierced mirror, as shown in Figure 5-6. The ASE is due to an inversion of population that occurs from the levels involving λ_{ni} = 546.1 nm and λ_{ni} = 404.7 nm transitions during the excitation pulse. The LDR for λ_{ni} = 546.1 nm is three orders of magnitude (from 1 ppb to 1 ppm), and could be extended by resorting to

Table 5-3. Results of the student t-test comparing the results of noise calculations made by a computer and manually made

Standard Deviation of the Blank Manually Calculated	Standard Deviation of the Blank Computer Calculated
4 25	3 78
3 06	3 47
3 14	3 63
3 28	3 81
3 73	2 9
3 03	4 58
4 65	4 21
Average (μ_1) 3.59	Average (μ_2) 3 77
Std Deviation 0 594	Std Deviation 0 495
F-test* (α = 0 05) H_0: $\sigma_m^2=\sigma_c^2$	1 44
F-value (α=0 05, 6, 6)	4 28
t-test (α=0 01) H_0. $\mu_1 = \mu_2$	2.1
t value (α = 0 01, 12)	3 1

* Checking the condition of homogeneity of variances. The condition of normality is assumed to be fullfilled

Figure 5-4. Calibration curves for λ_m=546.1 nm and λ_m=407.8 nm. The stray light noise level is for the measurement at λ_m=546.1 nm

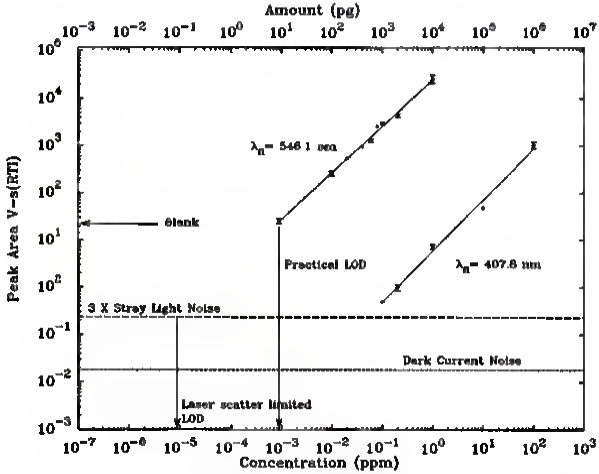
Amount (pg)
10^{-3} 10^{-2} 10^{-1} 10^{0} 10^{1} 10^{2} 10^{3} 10^{4} 10^{5} 10^{6} 10^{7}
Peak Area V-s(RTI)
10^{5} 10^{4} 10^{3} 10^{2} 10^{1} 10^{0} 10^{-1} 10^{-2} 10^{-3}
λ_n= 546.1 nm
λ_n= 407.8 nm
Blank
Practical LOD
3 X Stray Light Noise
Dark Current Noise
Laser scatter limited LOD
10^{-7} 10^{-6} 10^{-5} 10^{-4} 10^{-3} 10^{-2} 10^{-1} 10^{0} 10^{1} 10^{2} 10^{3}
Concentration (ppm)

Figure 5-5. Calibration curve for λ_{fl} = 546 1 nm. The line is the linear regression on the log data as calculated by Sigma Plot. The slope is 0 96 with r^2 = 0 99. The error bars are $\pm\sigma$. The last two points show the deviation due to ASE and are not included in the regression.

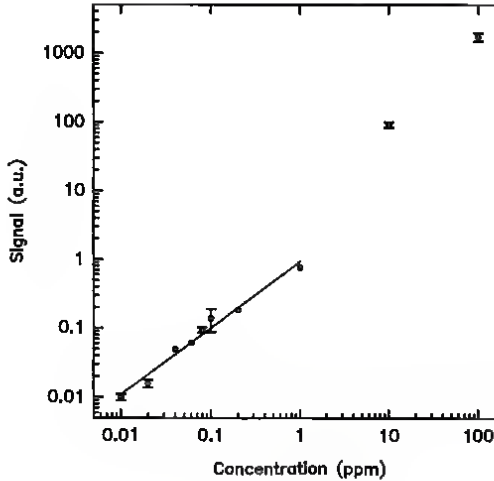
1000
100
10
1
0.1
0.01
Signal (a.u.)
0.01
0.1
1
10
100
Concentration (ppm)

Figure 5-6. Schematic diagram of the collection of fluorescence and ASE.

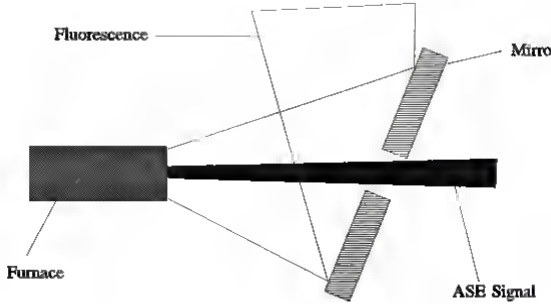
Fluorescence
Mirror
Furnace
ASE Signal

fluorescence measurements at the collisionally-coupled transition at λ_{03} = 407 8 nm where no inversion of population should occur, since the 7 $^3S_0$ level is about 1500 cm^{-1} above the 7 $^3S_1$ level and kT at the atomization temperature is only 1000 cm^{-1}.

Amplified Spontaneous Emission

Saturation Curves

Saturation was obtained for the first and second excitations steps, as shown by Figures 5-7 and 5-8 respectively The saturation energies were for λ_1 = 253 7 nm, ≈ 10 μJ, and for λ_2 = 435 8 nm, 15 μJ The error bars in both plots are given by $\pm\ \sigma$, where σ is the standard deviation of the triplicate analysis. The regression of the saturation curve of the first transition was calculated and plotted by Sigma Plot (v 5 1, Jandel Scientific, Corte Madera, CA) with a slope of 2 11 with r^2 = 0 992 The regression of the saturation curve of the second transition was calculated and plotted by Sigma Plot (v 5 1, Jandel Scientific, Corte Madera, CA), with a slope of 2 06 with r^2 = 0 996 The slopes can be explained by the intensity expression for ASE, equation 2-13, which predicts that for a gain length product (gL), of approximately one, the intensity will be proportional to the number density squared

It is worth noting that the cell used for this measurements shown an anomalous behavior for the dependence on buffer gas type. This anomalous behavior is described in the ASE Signal Dependence on Type of Buffer Gas section under the corresponding sub-section

Figure 5-7 Saturation curve for the first transition at $\lambda_1 = 253.7$ nm The line is the linear regression on the log data as calculated by Sigma Plot, and the error bars are $\pm\sigma$ of measurement. The slope is 2 11 with $r^2 = 0.992$ Data taken using anomalous cell (see text for explanation)

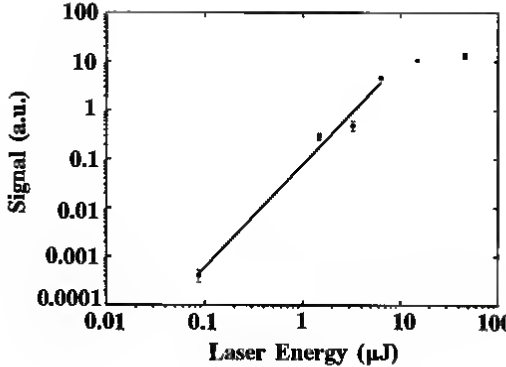
100
10
1
0.1
0.01
0.001
0.0001
Signal (a.u.)
0.01
0.1
1
10
100
Laser Energy (μJ)

Figure 5-8 Saturation curve for the second transition at $\lambda_1 = 435.8$ nm. The line is the linear regression on the log data as calculated by Sigma Plot. The slope is 2.06 with $r^2 = 0.996$. Data taken using anomalous cell (see text for explanation)

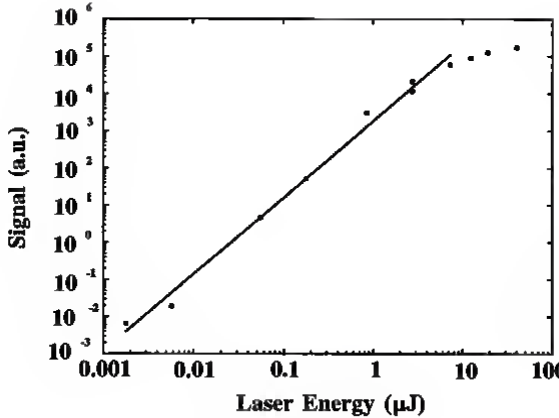
Signal (a.u.)
10 6
10 5
10 4
10 3
10 2
10 1
10 0
10 -1
10 -2
10 -3
0.001
0.01
0.1
1
10
100
Laser Energy (μJ)

ASE Signal Dependence on Mercury Number Density

The ASE signal dependence on mercury number density is presented in Figures 5-9 and 5-10 for vapor cell-II with argon as buffer gas, and cell-I with nitrogen as buffer gas (the anomalous behavior cell) Figure 5-11, presents the ASE signal dependence on number density for the graphite furnace with argon as buffer gas

Figure 5-9, clearly shows the amplifying behavior of the cell As described by theory, the signal increases much faster than the linear number density dependence of fluorescence. After this exponential dependence on the number density, the ASE signal reaches a plateau This plateau is reached because the ASE cannot grow indefinitely, and saturation will become important at this point. From a semi-log plot of the ASE signal versus number density, the calculated slope, αL (from equation 2-14), is $\approx 3\ 2 \times 10^{-13}$ cm^3 Using this number, a number density of 5×10^{13} atoms/cm^3, and substituting in equation 2-18, we find that the exponential term is $\approx e^{16}$ or 7×10^7, indicating that the medium is saturated

Using a simplified rate equation approach to describe the ASE mercury system as shown in Figure 5 12 we have the following equations:

$$\frac{dn_3}{dt} = R_3 - \frac{n_3}{\tau_3} - \rho_{32} I_{23}(n_3 - n_2) \tag{5-1}$$

where

Figure 5-9 ASE signal dependence on mercury number density, with 760 torr of argon as buffer gas. (cell-II) The error bars are $\pm\sigma$ of the measurement

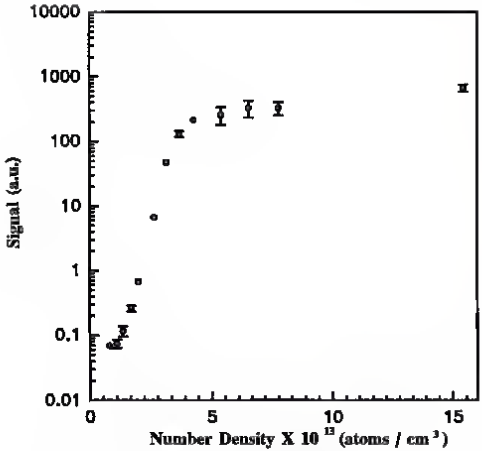
10000
1000
100
10
1
0.1
0.01
Signal (a.u.)
0
5
10
15
Number Density X 10 13 (atoms / cm 3)

Figure 5-10 ASE signal dependence on mercury number density for nitrogen at $\approx$ 500 torr as buffer gas. (cell-I) The error bars are $\pm\sigma$ of the measurement Data taken using anomalous cell (see text for explanation)

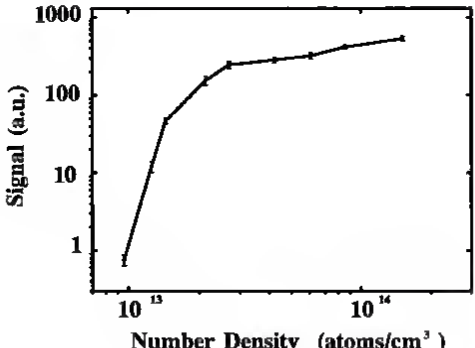
1000
100
10
1
Signal (a.u.)
10 13
10 14
Number Density (atoms/cm3)

Figure 5-11. ASE signal dependence on concentration for argon at 760 torr as buffer gas in the graphite furnace. The error bars are $\pm\sigma$ of the triplicate measurement.

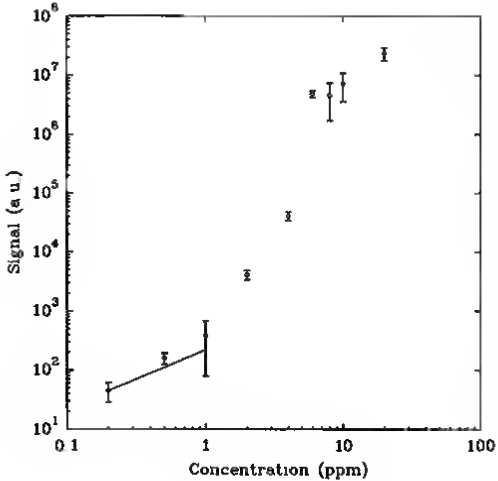
Signal (a.u.)
10^1
10^2
10^3
10^4
10^5
10^6
10^7
10^8
0.1
1
10
100
Concentration (ppm)

Figure 5-12 Simplified mercury energy level diagram Refer to text for explanations of symbols

1
2
3
R_3
$p_{32} I_{23}$
$p_{32} I_{32}$
k_{32}
A_{32}

$$\tau_3 = \frac{1}{\sum_{j<3} A_{3j} + \sum_{j<3} k_{3j}} \tag{5-2}$$

and where ρ_{23} is spectral energy density (J m^{-4}), I_{23} coefficient of stimulated emission (m^4 s^{-1} J^{-1}), A_{3j} are the Einstein coefficients of spontaneous emission (s^{-1}), k_{3j} are the collisional rates (s^{-1}), n_i are the level populations (m^{-3}), R_3 is the combined pumping rate for the lasers. The term $\rho_{23} I_{23}$ accounts for stimulated emission emerging from this transition. Assuming lasers with a square pulse of duration T and that $\rho_{32} = \rho_{23}$ and considering that at the beginning $I_{23} = 0$, we have

$$\frac{dn_3}{dt} = R_3 - \frac{n_3}{\tau_3} \tag{5-3}$$

Considering now, $I_{23} \neq 0$, $n_2 << n_1$, and steady state conditions gives:

$$\frac{dn_3}{dt} = 0 = R_3 - \frac{n_3}{\tau_3} - \rho_{32} I_{23}(n_3 - n_2) \tag{5-4}$$

and

$$\frac{dn_2}{dt} = 0 = R_2 + \frac{n_3}{\tau_{32}} - \frac{n_2}{\tau_2} + \rho_{32} I_{23}(n_3 - n_2) \tag{5-5}$$

where R_2 is the pumping rate of level 2 (only collisional), and

$$\tau_{32} = \frac{1}{A_{32} + k_{32}} \tag{5-6}$$

and

Deriving the population inversion, (n_3 - n_2) results in the following

$$\tau_2 = \frac{1}{\sum_{j<2} A_{2j} + \sum_{j<2} k_{2j}} \tag{5-7}$$

$$n_3 - n_2 = R_3 \tau_3 \left(1 - \frac{\tau_2}{\tau_{32}}\right) - R_3 \frac{\tau_2}{\left(1 + \frac{I_{22}}{I_{sat}}\right)} \tag{5-8}$$

where

$$I_{sat} = \frac{1}{\rho_{32} \tau_3} \frac{1}{\left(1 + \frac{\tau_2}{\tau_3} - \frac{\tau_2}{\tau_{32}}\right)} \tag{5-9}$$

The preceding equations have been derived to see the time evolution of level 3 and the conditions for which stimulated radiative rates becomes important between levels 3 and 2. From equation 5-9, one can see that stimulated emission shortens the lifetime of level 3 and that the population n_3 decreases when $I \approx > I_{sat}$. This helps to explain the behavior at the end of Figure 5-9 where a plateau is reached.

The same type of behavior is found for cell-1. In this case, the copper jacket that surrounded the cell did not allow cooling under 15°C. The calculated $\sigma L \approx 7.2 \times 10^{-13}$ cm^3. Making the substitutions into equation 2-18 gives $\approx e^{38}$ or 1.6×10^{15}. This also indicates saturation.

In the case of the graphite furnace, Figure 5-11 shows that for concentrations around 1 ppm the ASE starts to show. In the figure, the line shows where the normal fluorescence behavior will be if there is a linear dependence on density for the first three points. In the furnace with volume ≈ 0.79 cm^3 for 1 ppm, and assuming no loss, the

number density ≈ 3 6 x 10^{13} atoms/cm^3 Comparing this number density in Figure 5-9, this number coincided with the number density where the plot shows an abrupt increase

ASE Signal Dependence on Type of Buffer Gas

Normal cell behavior The results of the ASE dependence on buffer gas are presented in Table 5-4 The ASE signal for argon at atmospheric pressure is ≈ 3x higher than that for nitrogen, and ≈ 4.5x higher than the air signal From the slopes of the semi-log plots the cross sections are 3.2 x 10^{-14} cm^2 for argon, and 9 x 10^{-14} cm^2 for nitrogen. The cross section for nitrogen is ≈ 3 times higher than the one for argon In the case of nitrogen at atmospheric pressure it, is ≈ 1.5 x greater than that of the air.

Graphite furnace behavior The results for ASE dependence on argon and nitrogen as buffer gas in the graphite furnace are presented in Table 5-5. These results confirm that the argon ASE signal is ≈ 3x larger at atmospheric pressure.

Anomalous cell behavior The ASE from cell-I was found to be 10^5x higher than the others, and there is no explanation for this result This result was not reproducible with any other cell in the laboratory. The preparation and cleaning procedures for cell-I are unknown, and so a comparision with others cells cannot be made One major difference between this cell and the others is that the windows were glass blowed in the cell while in the others the were fixed with epoxy Another major difference is that this cell is completly galss sealed while the others use high vacuum stopcocks as seals

The ASE signal dependence on nitrogen pressure using cell-III was studied and is presented in the following section

Table 5-4 Buffer gas effect on ASE signal relative to that of the ≈500 torr of N_2

Buffer Gas	Gas Pressure (torr)	Relative Signal
Air	760	1.1×10^{-5}
N_2	760	1.55×10^{-5}
Ar	760	5.0×10^{-5}
N_2	≈ 500	1.0

Table 5-5 ASE signal dependence on type of buffer gas in the furnace The signal is relative to that for argon gas

Buffer Gas	Pressure (torr)	Relative Signal
Ar	760	1 0
N_2	760	0 32

ASE Signal Dependence on Nitrogen Pressure

The ASE signal dependence on nitrogen pressure is presented in Figure 5-13. The maximum signal was at ≈ 400 torr, and the maximum was only twice of that at 760 torr. This figure demonstrated that the ASE signal probably increased approximately with an increase of the absorption factor (shown in Figure 5-13 as calculated in Math-CAD by using equation 5-10) until other factors, such as collisions took over decreasing the signal. There is no explanation, though, for the behavior of cell-I, and only speculation can be made on the unknown preparation procedures for this cell.

$$k(\lambda) = \frac{B_{ij}\, n_i\, h\, \lambda\, S_\lambda}{c} \qquad (5\text{-}10)$$

where B_{ij} Einstein coefficient of stimulated absorption ($m^4\, J^{-1}\, s^{-2}$), n_i is the number density (m^{-3}), h is Planks constant ($J\, s$), λ is the wavelength (m), S_λ is the line profile (m^{-1}), and c is the speed of light.

Rate Equations Approach

The rate equations computer program was modified to calculate the theoretical saturation curve (see Appendix C). The saturation curves for the first and second transitions are presented in Figure 5-14 and 5-15, respectively. The saturation energy from this calculations were 3 μJ, and 5 μJ, for the first and second transitions, respectively.

Figure 5-13 ASE signal dependence (relative to the signal at 760 torr) on nitrogen pressure. The dashed line represents the absorption factor, as calculated by Math-CAD using equation 5-10 in the text.

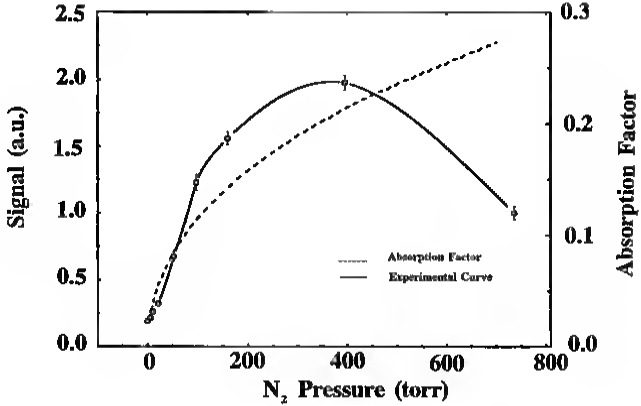
Signal (a.u.)
2.5
2.0
1.5
1.0
0.5
0.0
0.3
0.2
0.1
0.0
Absorption Factor
0
200
400
600
800
N_2 Pressure (torr)
Absorption Factor
Experimental Curve

Figure 5-14 Theoretical saturation curve for the first transition at λ_{41} = 546 1 nm, as calculated by the rate equations approach. The population of level four has been normalized to the total number density. The line is the linear regression on the log data as calculated by Sigma Plot, with slope m = 0 95 and r^2 = 0 999.

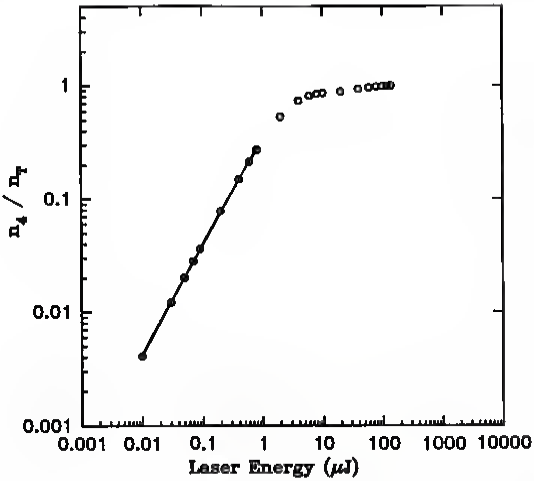
1
0.1
0.01
0.001
n_4 / n_T
0.001
0.01
0.1
1
10
100
1000
10000
Laser Energy (μJ)

Figure 5-15. Theoretical saturation curve for the second transition at $\lambda_{21} = 435.8$ nm, as calculated by the rate equations approach. The population of level four has been normalized to the total number density. The line is the linear regression on the log data as calculated by Sigam Plot, with slope $m = 0.95$ and $r^2 = 0.999$.

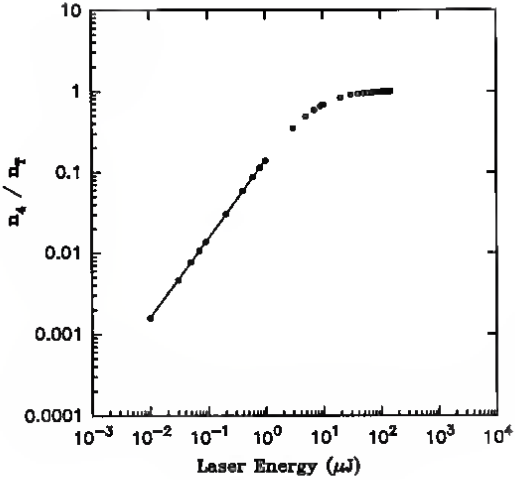
10
1
0.1
0.01
0.001
0.0001
n_4 / n_T
10^{-3}
10^{-2}
10^{-1}
10^{0}
10^{1}
10^{2}
10^{3}
10^{4}
Laser Energy (μJ)

Assuming that ASE is present and will vary as the square of the number density, the saturation plots calculated with the program were compared with the experimental saturation curves for ASE.

In Figures 5-16 and 5-17, the saturation curves for the first and second transitions, respectively are compared. In both cases good agreement was found between the theoretical and the experimental curves.

Figure 5-16. Comparison of the experimental saturation curve of the first transition for ASE, with the theoretical curve calculated by the rate equations approach. Note: ● experimental, ○ theoretical.

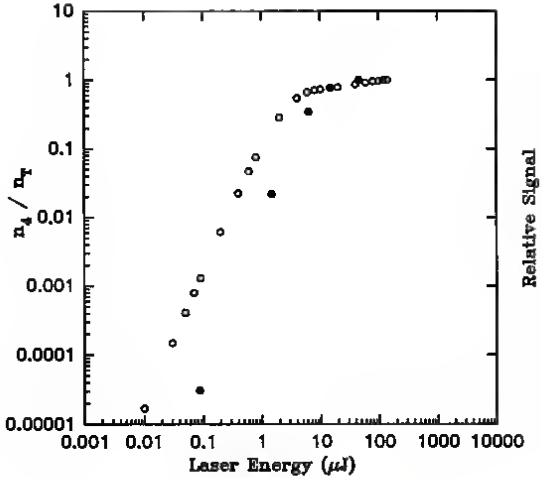
10
1
0.1
0.01
0.001
0.0001
0.00001
n_d / n_T
0.001
0.01
0.1
1
10
100
1000
10000
Laser Energy (μJ)
Relative Signal

Figure 5-17. Comparison of the experimental saturation curve of the second transition for ASE, with the theoretical curve calculated by the rate equations approach. Note ● experimental, ○ theoretical.

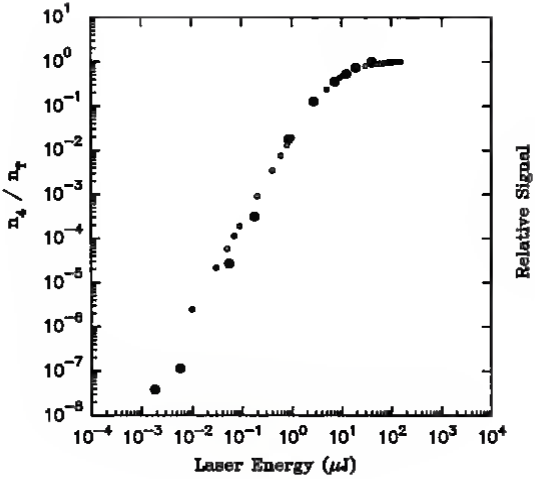
n_4 / n_T
10^1
10^0
10^{-1}
10^{-2}
10^{-3}
10^{-4}
10^{-5}
10^{-6}
10^{-7}
10^{-8}
10^{-4} 10^{-3} 10^{-2} 10^{-1} 10^0 10^1 10^2 10^3 10^4
Laser Energy (μJ)
Relative Signal

CHAPTER 6
CONCLUSIONS AND FUTURE WORK

Laser excited atomic fluorescence has been used for the determination of mercury with sub-pg instrumental detection limits The practical limit of detection was blank limited the best water in the laboratory contained about 1 ng/ mL of Hg The LDR for the 546 1 nm emission is approximately three orders of magnitude (from 1ppb to 1 ppm) and is limited due to a nonlinear amplified spontaneous emission process created by an inversion of population during the excitation pulse The LDR can be extended by using the collisionally-coupled transition at 407.8 nm

The use of LEAFS-ETA for the direct determination of mercury is promising especially with the excellent LODs and LDRs and the sample size required for measurement The need for better blanks is imperative for the usefulness of this technique, and so careful determination of the best water available and the best cleaning procedures, for this analysis should be done Future work includes the determination of mercury in samples of environmental importance and the study of this technique for different sample introduction conditions such as solids and slurries

The mercury fluorescence at λ_{em} = 546 1 nm has shown the ability to work as an amplified spontaneous emission amplifier or mirrorless laser For the first time ASE was observed for mercury vapor cells using a pulsed excitation The ASE at 546 1 nm was

observed for solutions concentrations higher or equal to one ppm in the furnace with nitrogen or argon as buffer gas, and number densities $> 10^{12}$ cm^{-3} in mercury vapor cells using nitrogen and argon as buffer gases. Saturation curves for the ASE were measured for both wavelengths of excitation. Both curves showed a square dependence on the energy of the respective laser. The dependence of the ASE on the number density was exponential for lower number densities, followed by a plateau due to the saturation of the gain.

Both the fluorescence and the ASE saturation curves were calculated using rate equations solved numerically by a computer. In the case of the ASE, the experimental and theoretical calculations were compared showing good agreement within experimental error.

Future work in this area could include be a more rigorous approach than the rate equation (e.g. density matrix) to describe the ASE phenomena. In that case, predictions of ASE in other atomic systems can be made, followed by the appropriate experimental investigations, in order to seek possible applications for this ASE mirrorless laser.

Also, the reproduction of the result for the anomalous cell is imperative. A detail study should be done of different preparation conditions as well as the possibility of opening the exciting anomalous cell to determine what is the composition of the buffer gas.

APPENDIX A
COMPUTER LISTING OF BASIC PROGRAM USED FOR THE NUMERICAL SOLUTION OF THE RATE EQUATIONS

```
REM
REM                    RATES.BAS
REM                         By
REM                   Dr. Denis Boudreaou
REM                         and
REM                   Wilfredo Resto-Otero
REM
CLS
pi = 3.141926#
F = 0
FOR J = 140 TO 200 STEP 20
      FOR C = 140 TO 140 STEP .02
REM
REM Initial populations and conditions
n0 = 1#
n1 = 0#
n2 = 0#
n3 = 0#
n4 = 0#
time = 0#
REM
REM  Degenaracies of states
REM
g0 = 1#
g1 = 1#
g2 = 4#
g3 = #
g4 = 3#
REM
REM Spontaneous Emission
REM
A20 = 1.3E+07
A42 = 4E+07
A43 = .6E+07
```

```
A41 = 1.8E+07
REM
REM Pressure of N2 buffer gas in torr
REM
P = 760
REM Collisional rates
REM
k20 = 620
k42 = 100000!
k43 = 700000 * P
k41 = 100000!
k32 = 3000000 * P
k21 = 114000!
k12 = 67
k10 = 18000!
REM
REM Laser Energies
REM
E1 = I * .000001
E2 = C * .000001
REM
REM Laser Diameters in mm
REM
d1 = 1
d2 = 2
REM
REM Rates of Stimulated Absorption and Emission (cm^-3) * ρ_ij
REM
L02 = (3.04E+11 * E1 * g2) / (g0 * pi * (.0 * d1) ^ 2)
L20 = (3.04E+11 * E1) / (pi * (.0 * d1) ^ 2)
L24 = (1.397E+13 * E2 * g4) / (g2 * pi * (.0 * d2) ^ 2)
L42 = (1.397E+13 * E2) / (pi * (.0 * d2) ^ 2)
REM
REM  Rates
REM
r20 = L20 + A20 + k20
r02 = L02
r10 = k10
r41 = A41 + k41
r21 = k21
r12 = k12
r42 = L42 + A42 + k42
r32 = k32
r24 = L24
```

```
r43 = A43 + k43
REM
REM File Name Creation
REM
F$ = "L_1 dat"
REM
REM Open Output File
REM
OPEN F$ FOR APPEND AS #1
REM
REM Calculations
REM
F = F + 1
iteration = 0
timeincrement = E-12
PRINT : PRINT : PRINT : PRINT "    Working in #:", F
100
IF time > 2E-08 THEN 200
      iteration = iteration + 1
      n0 = n0 + timeincrement * (r20 * n2 + r10 * n1 - r02
                                                  * n0)
      n1 = n1 + timeincrement * (r41 * n4 + r21 * n2 - (r10
                                                  + r12) * n1)
      n2 = n2 + timeincrement * (r02 * n0 + r42 * n4 + r32
                                                  * n3 + r12 * n1 - (r21 +
                                                  r24) * n2)
      o3 = n3 + timeincrement * (r43 * n4 - r32 * n3)
      n4 = n4 + timeincrement * (r24 * n2 - (r42 + r41 +
                                                  r43) * n4)
      time = time + timeincrement
      x = n0 + n1 + n2 + n3 + n4
      PRINT #1, time * E-9; n1 , n2 , n3 , n4 , x
         IF iteration <> 200 THEN 100
      iteration = 0
      GOTO 100
200
      CLOSE #1
      NEXT C
NEXT I
END
```

APPENDIX B
COMPUTER LISTING OF BASIC PROGRAM USED FOR THE CALCULATION OF INSTRUMENTAL NOISE FOR LEAFS-ETA

```
CLS   CLEAR 3000
t1 = TIMER
z = 0: c = 0: p = 0: i = 0: b = 0: ph = 0
INPUT "Please enter the total number of bins (max. 7000):", b
IF b > 100 THEN m = 1000
IF b > 1000 THEN m = 10000
PRINT
INPUT "Please enter the peak width in bin units", p
ph = INT(p * 1.5)
PRINT
INPUT "Please enter the file name.", F$
t2 = TIMER
t = t2 - t1
DO UNTIL t < .5
t = t / 2
LOOP
DIM n(100)
i = 1
DO UNTIL z > 100
10 n(i) = INT(RND(1) * t * m)
IF n(i) > b THEN 10
IF n(i) - ph < 1 THEN 10
IF n(i) + ph > b THEN 10
IF i = 1 THEN 20
c = 0
FOR j = 1 TO i - 1
        IF ABS(n(j) - n(i)) < INT(p *  .5) THEN c = 1
NEXT j
IF c = 1 THEN z = z + 1
IF c = 1 THEN i = i - 1
20 i = i + 1
LOOP
w = i
OPEN "NOISE.dat" FOR RANDOM AS #1
```

```
OPEN F$ FOR INPUT AS #2
FOR j = 1 TO b
INPUT #2, d, a
PUT #1, j, a
NEXT j
CLOSE
OPEN "cal.dat" FOR OUTPUT AS #1
FOR j = 1 TO w
        i = 0: ls = 0: rs = 0: ms = 0
        OPEN "noise.dat" FOR RANDOM AS #2
        e = (n(j) - ph)
        g = (n(j) - ph + p)
        FOR k = e TO g
                GET #2, k, s
                ls = ls + s
        NEXT k
        h = (n(j) + ph - p)
        o = (n(j) + ph)
        FOR k = h TO o
                GET #2, k, s
                rs = rs + s
        NEXT k
        bl = (ls / p + rs / p) / 2
        u = (n(j) - ph + p)
        v = (n(j) + ph - p)
        FOR k = u TO v
                GET #2, k, s
                ms = ms + s - bl
        NEXT k
        CLOSE #2
        y = y + ms
        PRINT ms
        WRITE #1, ms
NEXT j
CLOSE #1
yp = y / w
OPEN "cal.dat" FOR INPUT AS #1
FOR j = 1 TO w
        INPUT #1, ms
        vr = vr + ms ^ 2
        NEXT j
CLOSE #1

PRINT "STD. Deviation of blanks areas:"; SQR((vr - w * yp ^ 2) / w)
```

APPENDIX C
MODIFICATIONS TO COMPUTER PROGRAM LISTED IN APPENDIX A

```
REM
REM Calculations
REM
F = F + 1
iteration = 0
timeincrement = 5E-12
PRINT   PRINT : PRINT   PRINT "    Working in #;", F
100
IF time > 2E-08 THEN 200
      iteration = iteration + 1
      n0 = n0 + timeincrement * (r20 * n2 + r10 * n1 - r02
                                                  * n0)
      n1 = n1 + timeincrement * (r41 * n4 + r21 * n2   (r10
                                                  + r12) * n1)
      n2 = n2 + timeincrement * (r02 * n0 + r42 * n4 + r32
                                                  * n3 + r12 * n1 - (r21 +
                                                  r24) * n2)
      n3 = n3 + timeincrement * (r43 * n4 - r32 * n3)
      n4 = n4 + timeincrement * (r24 * n2 - (r42 + r41 +
                                                  r43) * n4)
      time = time + timeincrement
      IF iteration < > 200 THEN 100
      iteration = 0
      GOTO 100
200
      x = n0 + n1 + n2 + n3 + n4
      PRINT #1, J, n4/x
         CLOSE #1
      NEXT C
NEXT J
END
```

REFERENCE LIST

1. Alkemade, C Th.J., Milatz J M W., *Appl Sci Res*, 4B, 289 (1955)

2. Winefordner, J D., Vickers, T.J., *Anal. Chem*, 36, 161 (1964)

3. Ingle, J D, Jr., Crouch, S R., Spectrochemical Analysis, Prentince Hall, Inc., Englewood Cliffs, New Jersey (1988)

4. Butcher, D.J, Dougherty, J P, Preli, F R, Walton A P, Wei, G, Irwin, R L, Michel, R G, *J. Anal. At. Spectrom.*, 3, 1059 (1988)

5. Andrews, D L., Lasers in Chemistry, Springer-Verlag, New York (1986)

6. Svelto, O, Principles of Lasers, Plenum, New York (1982)

7. Schafer, F P, Editor, Dye Lasers, Springer-Verlag, New York (1973)

8. Smith, B W, Farnsworth, P B, Cavalli, P, Omenetto, N, *Spectrochim Acta*, 45B, 1369 (1990)

9. Vera, J.A., Leong, M.B., Omenetto, N, Smith, B W., Womack, B, Winefordner, J D, *Spectrochim Acta*, 44B, 939 (1989)

10. Vera, J A, Leong, M B, Stevenson, C L., Petrucci, G., Winefordner, J D, *Talanta*, 36, 1291 (1989)

11. Vera, J A, Stevenson, C L, Smith, B W, Omenetto, N, Winefordner, J D, *J Anal At Spectrom*, 4, 619 (1989)

12. Bolshov, M A, Zybinand, A V, Smirenkina, I I, *Spectrochim. Acta*, 36B, 1143 (1981)

13. Winefordner, J.D, Omenetto, N, *in* Piepmeier, E.H, Editor, Analytical Applications of Lasers, Wiley, New York (1986)

14. Omenetto, N, Winefordner, J D, *Prog Anal At Spectrosc*, 2, 1 (1979)

15 Omenetto, N , Editor, Analytical Laser Spectroscopy, Wiley, New York (1979)

16 Alkemade, C Th J , *in* Piepmeier, E H., Editor, Analytical Applications of Lasers, Wiley, New York (1986)

17 Alkemade, C Th J , *Spectrochim Acta B*, 40, 1331 (1985)

18 Omenetto, N , Human, H G C , *Spectrochim Acta B*, 39, 1333 (1984)

19 Martellucci, S , Chester, A N , Editors, Analytical Laser Spectroscopy, Plenum, New York (1985)

20 Winefordner, J D , *J Chem. Ed* , 55, 72 (1978)

21. Hieftje, G M , Editor, New Applications of Lasers to Chemistry, ACS Symposium Series No 85, American Chemical Society, Washington, DC (1978)

22. Falk, H , *Forg Anal. At. Spectrosc.*, 3, 181 (1980)

23 Hieftje, G M , Travis, J C , Lytle, F E., Editors, Lasers in Chemical Analysis, Humana Press, Clifton, New Jersey (1981)

24 Alkemade, C Th J , Hollander, Th , Snelleman, W , Zeegers, P J , Metal Vapors in Flames, Pergamon, London (1982)

25 Wei, G , Dougherty, J P , Preli, F R , Jr , Michel, R G , *J Anal At Spectrom* , 5, 249 (1990)

26 Dittrich, K , Stärk, H J, *J. Anal At Spectrom.*, 1, 237 (1986)

27 Swain, E B , Engstrom, D R., Brigham, M E , Henning, T A , Brezonik, P L., *Science*, 257, 784 (1992)

28 Lambou, V W , Mercury Technical Committee Interim Report, Center for Biomedical and Toxicological Research and Waste Management, Florida State University, Tallahassee, Florida (1991)

29 Lindqvist, O , *Water Air Soil Pollut* , 55, 1 (1991).

30 The Merck Index, Merck & Co , Rahway, New Jersey (1989)

31 Grosser, Z.A , *Environmental Testing & Analysis*, 1, 24 (1992)

32. Hatch, W R , Ott, W L., *Anal Chem* , 40, 2085 (1968)

33 Bushaw, B A , *Anal. Chem.*, 57, 2397 (1985)

34 Caupell, J.E , Hendrikse, P W , Bongers, J S , *Anal. Chim. Acta*, 81, 53 (1976)

35 Baxter, D C , Frech, W , *Anal. Chim. Acta*, 225, 175 (1989)

36 Grobenski, Z , Erler, W , Voellkopf, U , *At. Spectrosc* , 6, 91 (1985)

37 Powell, M J , Quan, E S K , Bakke, D W , Hughes, G H , *Anal Chem* , 64, 2253 (1992)

38 Smith, B W , Gluck, M R , Spears, K N , Winefordner, J D , *Appl. Spectrosc* , 43, 376 (1989)

39 Wiese, W L , Martin, G A , Wavelengths and Transition Probabilities for Atoms and Atomic Ions, NIST, Washington, D C (1980)

40 Siegman, A.E., Lasers, University Science Books, Mill Valley, California (1986)

41 Dicke, R H , *Phys. Rev.*, 93, 99 (1954)

42 Allen, L , Peters, G.I , *Phys Lett A*, 31, 95 (1970)

43 Bonifacio, R , Lugiato L.A , *Phys Rev A*, 11, 1507 (1975)

44 Bonifacio, R , Lugiato L A , *in* Bonifacio, R , Editor, Dissipative Systems in Quantum Optics, Springer-Verlag, New York (1982)

45 Bréchignac, C , Cahuzac, Ph , *J. Phys. B*, 14, 221 (1981)

46 Peters, G.I., Allen, L , *J. Phys. A*, 4, 238 (1971)

47 Allen, L , Peters, G.I , *J. Phys. A*, 4, 377 (1971)

48 Allen, L , Peters, G.I , *J. Phys. A*, 4, 564 (1971)

49 Allen, L , Peters, G.I , *J. Phys. A*, 5, 695 (1972)

50 Peters, G.I., Allen, L., *J. Phys. A*, 5, 546 (1972)

51 Allen, L , Peters, G.I , *Phys Rev A*, 8, 2031 (1973)

52 Casperson, L.W , *J. Appl Phys* , 48, 256 (1977)

53 Casperson, L W , Yariv, A , *IEEE J Quantum Electron* , 8, 80 (1972)

54 Maeda, H , Yariv, A , *Phys Lett. A*, 43, 383 (1973),

55 Ganiel, U , Hardy, A ,Neumann, G , Treves, D , *IEEE J Quantum Electron.* , 11, 881 (1975).

56 Wood, R W , *Philos Mag* , 50, 774 (1925)

57 Djeu, N , Burnham, R , *Appl. Phys. Lett* , 25, 350 (1974).

58 Holmes, N C , Stegman, A E., *J Appl Phys* , 49, 3155 (1978)

59 Daily, J W , *Appl. Opt* , 16, 2322 (1977)

60 Daily, J W , *Appl. Opt* , 17, 225 (1978)

61 Van Dijk, C A , Omenetto, N , Winefordner, J D , *Appl Opt* , 35, 389 (1981)

62 Piepmeier, E.H., *Spectrochim. Acta*, 27B, 431 (1972).

63 Piepmeier, E.H., *Spectrochim. Acta*, 27B, 445 (1972),

64 Omenetto, N., Smith, B W , Hart, L P , *Fresenius Z. Anal Chem* , 324, 683 (1986)

65 Ayala, N L, Resonance Line Lasers as Excitation Sources for Atomic Spectrometry, Ph.D. dissertation, Department of Chemistry, University of Florida, Gainesville, (1992)

66 Rettberg, T.M., Beach, L M , *J Anal At Spectrom* , 4, 427 (1989)

67 Del Angel, G A , Coq, B , Ferrat, G , Figeras, F., *Surf Sci* , 156, 943 (1985).

68 Sudhakar, C , Vannice, M A , *Appl Catal* , 14, 47 (1985).

69 Gillet, E., Channakhone, S , Matolin, V , *J Catal.* , 97, 437 (1986)

BIOGRAPHICAL SKETCH

Wilfredo Resto-Otero was born in Bronx, New York, on December 12, 1966. In May, 1989, he graduated from the University of Puerto Rico, Colegio Universitario de Cayey, Cayey, Puerto Rico, with a Bachelor of Science degree with a major in chemistry. He was vicepresident of the Chemistry Society at Colegio Universitario de Cayey from 1987-1988 and president from 1988-1989. He was a member of the organization committee of Techno-Chem '89, the first technological meeting and exposition at Colegio Universitario de Cayey. He participated in summer undergraduate research programs at New Mexico State University, the University of New Mexico and Florida State University. In August, 1989, he entered the Graduate School at the University of Florida in Gainesville.

He is a member of the American Chemical Society, the Society for Applied Spectroscopy, and the Puerto Rico Chemists Association.

I certify that I have read this study and that in my opinion it conforms to acceptable standards of scholarly presentation and is fully adequate, in scope and quality, as a dissertation for the degree of Doctor of Philosophy.

James D. Winefordner, Chairman
Graduate Research Professor of
Chemistry

I certify that I have read this study and that in my opinion it conforms to acceptable standards of scholarly presentation and is fully adequate, in scope and quality, as a dissertation for the degree of Doctor of Philosophy.

Richard A. Yost
Professor of Chemistry

I certify that I have read this study and that in my opinion it conforms to acceptable standards of scholarly presentation and is fully adequate, in scope and quality, as a dissertation for the degree of Doctor of Philosophy.

David H. Powell
Associate Scientist of Chemistry

I certify that I have read this study and that in my opinion it conforms to acceptable standards of scholarly presentation and is fully adequate, in scope and quality, as a dissertation for the degree of Doctor of Philosophy.

John R. Eyler
Professor of Chemistry

I certify that I have read this study and that in my opinion it conforms to acceptable standards of scholarly presentation and is fully adequate, in scope and quality, as a dissertation for the degree of Doctor of Philosophy.

Eric R. Allen
Professor of Environmental
Engineering Sciences

This dissertation was submitted to the Graduate Faculty of the Department of Chemistry in the College of Liberal Arts and Sciences and to the Graduate School and was accepted as partial fullfillment of the requirements for the degree of Doctor of Philosophy.

December, 1993

Dean, Graduate School